ORIGINAL RESEARCH COMMUNICATION

Elucidation of the AGR2 interactome in esophageal adenocarcinoma cells identifies a redox sensitive chaperone hub for the quality control of MUC-5AC.

Jack C. Worfolk[1], Steven Bell[1], Lee D. Simpson[1], Naomi A. Carne[1], Sarah L. Francis[1], Vibecke Engelbertsen[2], Adrian P. Brown[1], Julie Walker[2], Yirupaiahgari K Viswanath[2] and Adam M. Benham[1*]

From the [1]Department of Biosciences, Durham University, Stockton Road, Durham, DH1 3LE, UK; [2] Department of Surgery, James Cook University Hospital, Marton Road, Middlesbrough TS4 3BW, UK

Running title: *The AGR2 interactome in esophageal adenocarcinoma*

*To whom correspondence should be addressed: Adam Benham, Department of Biosciences, Durham University, Stockton Road, Durham, DH1 3LE, UK. Tel: +44 (0)191 334 1259. FAX: +44 (0)191 334 1201. Email adam.benham@durham.ac.uk

Word count (excluding abstract, references and legends): 7,301

References: 41

Grayscale illustrations: 6

Color illustrations: 2

Keywords: Protein Disulfide Isomerase, Endoplasmic Reticulum, chaperone, redox, mucin, cancer.

Abstract

***Aims**:* AGR2 is a tissue-restricted member of the Protein Disulfide Isomerase family that has attracted interest because it is highly expressed in a number of cancers, including gastro-esophageal adenocarcinoma. The behaviour of AGR2 was analysed under oxidising conditions and an alkylation trapping and IP approach was developed to identify novel AGR2 interacting proteins.

***Results**:* The data show that AGR2 is induced in esophageal adenocarcinoma, where it participates in redox responsive, disulfide-dependent complexes. AGR2 preferentially engages with MUC-5 as a primary client and is co-expressed with the acidic mucin in Barrett's esophagus and esophageal adenocarcinoma tissue.

Innovation: New partner chaperones for AGR2 have been identified, including Prx-IV, ERp44, P5, ERp29 and Ero1α. AGR2 interacts with unexpected metabolic enzymes including ALDH3A1 and engages in an alkylation-sensitive association with the autophagy receptor SQSTM1, suggesting a potential mechanism for the post-ER targeting of AGR2 to mucin granules. Disulfide-driven AGR2 complex formation provides a framework for a limited number of client proteins to interact, rather than for the recruitment of multiple novel clients.

Conclusion: The extended AGR2 interactome will facilitate the development of therapeutics to target AGR2/mucin pathways in esophageal cancer and other conditions, including chronic obstructive pulmonary disease.

Introduction

AGR2 is a small 19 kDa, tissue restricted chaperone that is distantly related to the PDI family of disulfide isomerases. AGR2 was first described in *Xenopus laevis* as XAG-2 (1), where it controls dorsoanterior ectodermal fate and is required for the establishment of the cement gland. The mammalian homolog, AGR2, was cloned from murine intestinal goblet cells and was initially named gob4 (17). AGR2/gob4 has subsequently been shown to be required for the correct folding and secretion of cysteine-rich mucins, the large glycoproteins that give mucus its viscosity. The importance of AGR2 in gastro-intestinal biology

was demonstrated in an AGR2 deficient mouse, in which the animals develop a form of colitis as a result of insufficient mucus secretion in the intestine (25). Diminished expression of AGR2 in *Agr2*$^{-/-}$ mice also results in an ER stress response that contributes to inflammatory bowel disease (39). Although AGR2 is required for mucin disulfide bond formation, the mechanism by which it performs this function is enigmatic, as AGR2 possesses only one cysteine residue (C81) in its solitary thioredoxin-like **a** domain (residues CPHS). It is not known whether AGR2 can discriminate between different mucin protein clients or whether AGR2 is required for the secretion and quality control of all types of mucins. Determining how AGR2 controls the secretion of the stomach and airway mucins (2), as well as other potentially unknown clients, is therefore an important unresolved issue.

AGR2 was initially shown to be co-expressed with the estrogen receptor in several breast cancer cell lines, suggesting a possible role in breast cancer biology (35). Subsequently, de-repression of AGR2 was discovered in a variety of adenocarcinomas including those of the prostate (38), esophagus (28), pancreas (29), ovary (24) and lung (41). The elevated expression of AGR2 in a range of cancer tissues has sparked interest in AGR2 as a potential biomarker for cancer progression, and it is an attractive target for "broad-spectrum" therapies designed to target multiple key pathways and mechanisms in cancer (6). The biological advantage that AGR2 expression confers to cancer cells has been the subject of debate; AGR2 expression correlates with an increase in cell growth, proliferation (28), adhesion and metastasis (19), whereas Sommerova et al have suggested that AGR2 contributes to the maintenance of a tumour cells epithelial phenotype and is downregulated by TGFβ in a range of cancer cell lines (34). AGR2 normally resides in the ER of cells, is induced by the ER stress response and contributes to ER homeostasis (12). However, AGR2 has an unconventional KTEL ER-retention/retrieval sequence and can be found in the extracellular matrix (9) or at the plasma membrane, particularly in late-stage cancer cells (11). In this environment, AGR2 can recruit growth factors such as AREG, an EGFR ligand, to promote cancer cell survival and proliferation (8). Elevated expression of mucins in adenocarcinomas, whose quality control is facilitated by AGR2, may therefore encourage the entrapment of pro-oncogenic growth factors (37).

The NMR structure of AGR2 has been solved and reveals an unstructured N-terminal region from residues 21-40 followed by a C-terminal thioredoxin fold that homodimerises through salt bridges (27). Residues E60, Y63 and K64 are required for dimerisation at the α1 helix, but the C81 residue, which could potentially be involved in homodimer formation, is not required for AGR2 self-association. *In vitro*, the AGR2 protein has a monomer-dimer distribution with a dissociation constant of 8.83 μM in phosphate/sodium chloride at pH 6.5. The NMR data suggests that the unstructured N-terminal domain of AGR2 interacts with clients such as cell adhesion proteins. However, an independent study has shown that a peptide loop in AGR2 at residues 131-135 in the thioredoxin domain can interact with the peptide sequence TTIYY (21). Thus the sequence specificity and mechanism by which AGR2 interacts with associating proteins in the secretory pathway and beyond requires further investigation.

Interactome studies to establish PDI family client profiles have been successfully undertaken and demonstrate that PDIs have a degree of substrate specificity. PDIA3 (ERp57), for example, preferentially engages with proteins containing small disulfide rich domains (13) and the complex between PDIA3 and tapasin has also been characterised using a thiol modification approach (3). PDIA6 (P5) has specificity for clients of the ER resident Hsp70 protein BiP (14). PDIp, the pancreatic acinar cell PDI homolog, interacts with αamylase and a set of proenzymes, including proelastase (10), whereas the testis-specific PDILT is required for the processing of the sperm adhesion protein ADAM3 (36). Most interaction studies have required transfection of tagged PDIs with the CXXC motif mutated to CXXS, to enable client trapping by alkylation, which prevents disulfide-bond rearrangements. However, a mutagenesis strategy may perturb the ER redox poise or the ER protein load, leading to potential interactions with off-pathway proteins. An alternative method of co-IP followed by immunoblotting to detect likely interactors may lead to biased and incomplete identification of clients. Here, these issues have been circumvented by exploiting the solitary cysteine residue in the AGR2 protein to establish the disulfide-dependence of AGR2 interactions. Using an alkylation-trapping approach, we aimed to identify the native client profile of a key PDI family member under both normoxic and oxidising conditions. The results lead us to propose a model for AGR2

in which the protein recruits co-chaperones, disulfide isomerases and oxidoreductases for MUC-5AC and MUC-5B quality control and onward transport from the ER.

Results

AGR2 is derepressed in OE19 adenocarcinoma cells

In previous work, we studied the behaviour of the ER oxidoreductase Ero1α in esophageal adenocarcinoma cells and showed that Ero1α was upregulated in pre-malignant Barrett's epithelium and esophageal adenocarcinoma (4). Given that the ER controls the secretion of extracellular proteins required for metastasis and survival, we investigated the expression of a range of other ER chaperones in the esophageal cell lines OE19 and OE33 to identify candidate proteins for further study (Figure 1). SDS-PAGE and western blotting revealed that most ER chaperones, including PDI, calnexin and Prx-IV were expressed similarly in the two cell lines (Figure 1, panels 2-5). ERp29 was mildly elevated by ~1.5 fold (by densitometry) in OE19 cells. In contrast, AGR2 was very strongly expressed in OE19 cells and was not detectable by western blotting in OE33 cells (Figure 1, top panel).

AGR2 engages in redox responsive disulfide-bonded complexes

Having established that OE19 cells express high levels of AGR2, we used this cell line to investigate the behaviour and function of AGR2 without the need for ectopic expression by transfection. The single cysteine residue (Cys81) in AGR2 is reported to form mixed disulfide bonds with MUC-2 (25), but its role in homodimerization of AGR2 has been disputed (32). With this in mind, we investigated whether redox-inducible disulfide-dependent AGR2 complexes could be visualised through non-reducing SDS-PAGE and western blotting. Thus OE19 cells were treated for 0, 5 or 10 min with diamide, which oxidises glutathione and other free thiols and promotes disulfide bond formation (18). The cells were lysed in the presence of the alkylating agent NEM to prevent disulfide bond reshuffling during analysis (Figure 2A, schematic). The samples were separated by both non-reducing and reducing SDS-PAGE, to

detect disulfide dependent complex formation, and analysed by western blotting with the D9V2F AGR2 mAb.

The results of a representative experiment show that rapid induction of AGR2 complexes by diamide could be detected under non-reducing conditions (Figure 2B, compare lanes 4 and 5). Multiple bands were visible at higher molecular weights (~75-250 kDa) along with a distinct band appearing at ~37 kDa, which is likely to be AGR2 in its homodimeric form (32). These AGR2 complexes were disulfide dependent as they were dispersed by the addition of the reducing agent DTT to the sample buffer (Figure 3B, compare lanes 2 and 3 with lanes 5 and 6). Diamide did not induce a change in the steady-state expression level of the ~20 kDa AGR2 monomer (Figure 2B, lanes 1-3). These results demonstrate clearly that endogenous AGR2 can form redox and disulfide bond dependent complexes at steady-state with partner proteins through a solitary cysteine residue when the ER becomes oxidising.

A recovery experiment was performed to determine whether the AGR2 complexes induced by diamide were stable or transient. Following a 5 min treatment with 5 mM diamide, OE19 cells were exposed to diamide-free media for 5, 10 or 20 min before alkylation and lysis, as previously described. Disulfide dependent complexes were induced rapidly after treatment with diamide, consistent with Figure 2B (Figure 2D, lane 7). After 20 min recovery, many bands persisted (Figure 2D, lanes 8-10), demonstrating that transient changes to the glutathione and free thiol pool resulted in resilient changes to the AGR2 interactome. A number of complexes did disappear, including a ~50 kDa complex (Figure 2D, *, lane 7) above the dimer band (~37 kDa) in the 5 min treatment that was absent in the recovery lanes. Actin was used as a blotting control (Figure 2C and 2E). These results show that under oxidising conditions, AGR2 can form a range of complexes with varying degrees of stability.

Identification of the redox-responsive AGR2 interactome

The appearance of AGR2 complexes under oxidising conditions could reflect the recruitment of a large number of novel or inducible AGR2 interacting proteins or the complexes could arise from multiple AGR2 molecules being recruited to a smaller set of interacting protein(s). To identify AGR2 interactors

and to address whether these complexes are the result of interactions with different sets of proteins, mass spectrometry was used to classify the redox-responsive AGR2 interactome. To validate the approach, IP was performed on alkylated lysates from diamide treated OE19 cells with the ab76473 AGR2 mAb. IPed samples were subjected to reducing western blotting with the independent D9V2F AGR2 mAb to confirm AGR2 recovery. The AGR2 monomer band in the 20 kDa region was evident in both the input (Figure 3, lanes 1 and 2) and the AGR2 IP lanes (Figure 3, lanes 4 and 5), and was entirely absent in the control IgG-only lane (Figure 3, lane 3), demonstrating that AGR2 could be efficiently retrieved and that diamide and NEM did not interfere with antibody recognition of AGR2.

Next, we analysed AGR2 IP samples with ESI mass spectrometry, to determine the identities of the protein components of the AGR2 complexes. As before, OE19 cells were treated +/- diamide, alkylated, lysed and IPed, then eluted and trypsin digested. As a control, trypsin digests of mock IPed samples were also performed. The identified peptides were tabulated (Tables 1, 2 and supplementary data), excluding the non-specific proteins from the control IP and any known contaminant peptides that were identified in the negative control (keratin, tubulin, albumin, trypsin, immunoglobulin, Hsp70, Hsp90, actin, elongation factors and histones; supplementary data). Identifications of potentially specific interacting partners from Mascot and ProteinPilot analysis were judged to be authentic if two or more peptide matches were obtained at 95% confidence. High peptide coverage was obtained for AGR2 (65% coverage at 95% confidence in the diamide samples and 41% coverage at 95% confidence for the non-diamide samples). The related AGR3 protein could not be detected by mass spectrometric analysis of OE19 cell lysates and no unique AGR3 peptide sequences were detected after IP, with the AGR2 antibody, demonstrating the specificity of the IP for AGR2 and not AGR3.

The mucins MUC-5AC and MUC-5B were the principle client proteins detected with high peptide coverage (MUC-5AC: 12% coverage –diamide and 23% coverage + diamide; MUC-5B: 7% coverage – diamide and 27% coverage + diamide). Although a quantitative proteomic approach to count relative peptide abundance was not used, the increase in peptide coverage following diamide treatment suggests that oxidising conditions enhance the recruitment of AGR2 to MUC-5AC and MUC-5B. Previous studies

have shown that AGR2 preferentially binds to mucins and associates with MUC-2 (25) as well as MUC-5AC and MUC-5B (33). Analysis of mass spectrometry data from OE19 and OE33 cell lysates revealed that MUC1, MUC5, MUC12 and MUC 13 were expressed in OE19 cells whereas only MUC20 was detectable at low peptide counts in OE33 cells (Table 3). This data is consistent with the hypothesis that AGR2 does not associate with every mucin and suggests that AGR2 upregulation is not required for the production of MUC20. Taken together, these results highlight a primary role for AGR2 in the quality control of MUC-5AC and MUC-5B in adenocarcinoma cells and suggest that an oxidising ER promotes AGR2 recruitment to specialist clients, rather than wholesale changes in the AGR2 client interactome.

Other significant protein interactions were detected between AGR2 and the ER chaperones GRP78/BiP (22-31% peptide coverage), calnexin, the peptidyl-prolyl cis-trans isomerase PPIA, four members of the PDI family (ERp29, PDIA3 (ERp57), PDIA6 (P5), ERp44) and two other ER proteins involved in disulfide bond formation, Ero1α and Prx-IV. The results indicate that AGR2 interacts with redox-active ER-resident chaperones to facilitate mucin quality control and show that the recruitment of ERp44, P5 and Ero1α to AGR2 occurs under oxidising conditions. The interaction between AGR2 and BiP has previously been demonstrated (32) confirming the validity of the approach; however, an association between AGR2 and the other chaperones listed in Tables 1 and 2 has not, to our knowledge, been reported. Novel associations between AGR2 and less well-characterised proteins were also detected, including metabolic enzymes (e.g. ALDH3A1), prostaglandin reductase 1 (PTGR1), transgelin-2 (TAGLN2), annexin A2, the cargo receptor BCAP31, the 14-3-3 zeta/delta adapter protein (YWHAZ) and the vesicle trafficking protein VAPA (Tables 1, 2 and supplementary data). Detection of the interaction between AGR2 and PTGR1, VAPA and BCAP1 was dependent on the presence of diamide. The data indicates that these protein-protein interactions are redox responsive. To confirm the interaction between AGR2 and one of the unexpected non-ER resident proteins, ALDH3A1, an IP was performed on OE19 lysates using an ALDH3A1 antibody and the IPs were analysed by mass spectrometry (Table 4). AGR2 was detected in the ALDH3A1 IPs. These new interactions provide a foundation for future mechanistic studies of AGR2 and its post-ER targeting and trafficking.

AGR2 interacts with MUC-5AC and a hub of ER chaperones, including Grp78/BiP, Prx-IV and ERp44

In order to validate the mass spectrometry data, a selection of AGR2 interacting proteins, which had been identified with both high and low percentage coverage, was confirmed by western blotting of IP samples. AGR2 IPs from OE19 lysates were prepared independently as described previously (+/- diamide with alkylation) and samples were analysed under reducing conditions. MUC-5AC was successfully detected after AGR2 IP and was more prominent in the sample from diamide treated cells (Figure 4A, lanes 2 and 3) verifying its association with AGR2 and supporting the idea that oxidising conditions drive the recruitment of AGR2 to MUC-5AC. The signal appeared as multiple banding covering a range of high molecular weights, as expected for a heterogenous glycoprotein. When immunoblotting for BiP a faint signal was detected, showing that an association occurred between AGR2 and BiP in the presence of diamide (Figure 4B, first panel). The novel AGR2 interactors ERp44 and Prx-IV were also detected by western blotting after AGR2 IP (Figure 4B, second and third panel). Both ERp44 and Prx-IV were only prominent in the diamide IP samples, indicating that oxidising conditions promote these chaperone associations.

To establish the dependence of oxidising conditions for the AGR2 interactome, and to control for the possibility that the AGR2 antibody might bind non-specifically to the other PDI proteins, OE19 and OE33 cells were cultured in the absence of diamide and lysed prior to AGR2 IP and analysis of the IPs by mass spectrometry. The data are presented in Tables 5 and 6. The interaction between AGR2 and MUC-5 in OE19 cells persisted during “normoxic” conditions, whereas the interaction between AGR2 and ER chaperones was below the limit of detection, supporting the idea that oxidising conditions promote the recruitment of accessory chaperone and folding factors to AGR2. Some AGR2 could be detected in OE33 IPs, despite AGR2 being undetectable in these cells by Western blotting (Figure 1), thus demonstrating the sensitivity of the mass spectrometric approach. The absence of PDI family proteins in the OE33 AGR2 IPs, confirmed that the AGR2 antibody did not bind non-specifically to these proteins.

An alkylation-sensitive interaction between AGR2 and the oxidative stress sensor SQSTM1/p62

Analysis of the data presented in Table 4 revealed that, in the absence of NEM, AGR2 interacted with SQSTM1 with high confidence and with broad peptide coverage of 18%. This interaction was lost upon alkylation, was not detected in OE19 cells that had been exposed to diamide (Tables 1 and 2) and was not detected in the $AGR2^{low}$ OE33 cells (Table 6). To independently validate this interaction, OE19 cells were lysed +/- NEM. The lysates were IP'ed with the anti-AGR2 antibody (ab76473) and subjected to western blotting to detect SQSTM1 (Figure 5A). The membrane was stripped and reprobed to detect actin and IgG as blotting controls (Figure 5B). Figure 5 demonstrates that SQSTM1 associated with AGR2 in the absence of NEM only. SQSTM1 is a cysteine-rich protein that can deliver protein complexes to the autophagosome (23), links redox state to proteostasis (7) and interacts with KEAP1 to control the transcriptional response to oxidative stress in cancer cells (16). It will be very interesting, therefore, to determine how AGR2 is involved in the delivery of client proteins to autophagosomes or other vesicles in both normal goblet cells and in adenocarcinoma.

Co-localization of AGR2 with Prx-IV and ALDH3A1 in esophageal cancer cells

AGR2 interacted with the MUC-5AC client, ER chaperones and some non-ER resident proteins. Thus the intracellular distribution of AGR2 was investigated to determine whether or not the protein was predominantly ER localised in OE19 cells. To ascertain the distribution of AGR2 by immunofluorescence, OE19 cells were grown on coverslips, fixed, permeabilised with Triton X-100 and co-stained for AGR2 and the ER marker PDI (Figure 6A), the Golgi marker GM130 (Figure 6B), the AGR2 interacting ER chaperone Prx-IV (Figure 6C), the AGR interacting non-ER localised aldehyde reductase ALDH3A1 (Figure 6D) and the AGR2 client MUC5 (Figure 6E). AGR2 predominantly overlapped with the ER marker PDI and showed no co-localisation with GM130, as expected. MUC-5AC and Prx-IV co-localised with the majority of AGR2 in the ER; ALDH3A1 was enriched in heterogenous clusters throughout the cytoplasm (Figure 6D, arrows) and co-localised with a smaller pool of AGR2 molecules (Figure 6D, asterix). The ER and cytoskeleton could also be clearly distinguished in the OE19 cells, as judged from

the discrete staining of the ER (PDI) and tubulin (Figure 6F). Taken together, the data indicate that at steady state, the majority of AGR2 resides in the ER of OE19 cells, with a smaller pool distributed beyond the ER and absent from the Golgi.

AGR2 interacts with MUC-5AC in esophageal adenocarcinoma and is co-expressed with MUC-5 in Barrett's esophagus and esophageal adenocarcinoma tissue

To apply the findings from OE19 cells to human disease, we turned to the gastro-intestinal tract and investigated whether the interaction between AGR2 and the major client MUC-5AC (Tables 1 and 2) could be detected *in vivo*. Esophageal adenocarcinoma tissue and normal tissue taken from an adjacent site were lysed +/- NEM and subjected to AGR2 IP followed by western blotting to detect MUC-5AC. Figure 7A and B shows that AGR2 and MUC-5AC were strongly co-expressed in the adenocarcinoma tissue and were not detectable in the normal epithelia. MUC-5AC co-IPed with AGR2 in the adenocarcinoma, demonstrating the capacity of the cell-line proteomic approach to reveal *bone fide in vivo* protein-protein interactions (Figure 7C). Note that Coomassie stained lysates were used as a control because the level of actin was lower in the adenocarcinoma tissue (Figure 7D and supplementary western blot data). The AGR2 interaction with MUC-5AC occurred in the presence or absence of NEM corroborating the results from the OE19 cells (Tables 1, 2 and Figure 4). Interestingly, in the presence of NEM, the interaction between AGR2 and the higher molecular weight forms of mucin were preferentially captured (Figure 7C, compare lane 2 with lane 4).

The transition from normal esophageal tissue to esophageal adenocarcinoma is accompanied by changes in tissue morphology and mucin expression and is frequently preceded by Barrett's esophagus. To test whether MUC-5AC and other novel AGR2 interacting proteins were also expressed and co-localised in the pathological GI tract, Barrett's esophageal and adenocarcinoma tissue sections were stained for AGR2 (with the D9V2F AGR2 antibody), MUC-5AC, Prx-IV and SQSTM1. The same tissue blocks were used to sequentially stain for each protein, with corresponding negative controls. Representative results from one of three blocks are shown in Figure 8 and duplicate and triplicate stainings from N=3

independent tissue sections (to demonstrate reproducibility across different individual tissues) are shown in the supplementary data (supplementary Figures 1 and 2). All four proteins were strongly expressed in the dysplastic goblet cells (brown staining). AGR2 and MUC-5AC expression was restricted to the goblet cells and was not seen in the surrounding epithelium (Figure 8A and B). The co-localisation of AGR2 and MUC5-AC in intestinal dysplasia was further confirmed by immunohistochemistry of 3 more independent Barrett's esophagus sections, and low magnification images of these co-stainings are shown in supplementary Figure 3. AGR2 also co-localised with alcian blue staining for acidic mucins in Barrett's esophagus and adenocarcinoma tissue; AGR2 and acidic mucins were not expressed in normal esophageal epithelium, as expected (supplementary Figure 4). SQSTM1 and Prx-IV were enriched in the goblet cells of both Barrett's epithelium and adenocarcinoma and were also present in the surrounding epithelium (Figure 8C and D). These results validate the OE19 experimental model and demonstrate that there is strong induction of AGR2 and MUC-5AC in malignant and pre-malignant esophageal tissue. Taken together, these findings open up the AGR2 interactome to screen for novel biomarkers of human GI disease.

Discussion

In this work, over 20 new AGR2 interacting proteins have been identified from esophageal cancer cells (Tables 1 and 2). At least eight of these proteins are ER chaperones/folding factors, with just one major secretory protein client identified, MUC-5AC/B. AGR2 is important for the quality control of mucous secretion and is strongly upregulated in various cancers, but it is unclear whether AGR2 functions as an isomerase *in vivo*, given that it is a PDI homolog that lacks a fully functional CXXC motif. The data in this paper shows that AGR2 can form higher molecular weight complexes in a disulfide dependent way under oxidising conditions (Figure 2). This result shows that a protein disulfide isomerase with a solitary cysteine residue can be redox responsive, and it will be interesting to revisit NMR studies (27) to determine whether changes in redox conditions *in vitro* result in changes to the structural properties of AGR2. An unresolved question in the field is whether C81 is required for the well-known

homodimerisation of AGR2. We show that AGR2 C81 mediates more than just AGR2-AGR2 dimerisation, and that AGR2 likely uses this residue to interact with other protein partners (Figure 2). The data support a model in which AGR2 is recruited to MUC-5AC and MUC-5B under normoxic conditions. If the environment becomes more oxidising, more AGR2 monomers are likely to bind MUC-5AC and MUC-5B through Cys81 and a non-covalent interaction with the unstructured N-terminal domain. AGR2 may protect exposed cysteine residues in MUC5-AC, limiting the number of off-pathway misfolding options, and enabling the much larger, multi-disulfide bonded MUC5-AC client to fold.

The finding that AGR2 interacts with other redox-active PDI family members such as the calnexin cycle reductase PDIA3/ERp57 (Tables 1 and 2), both in the presence or absence of diamide, suggests that AGR2 may facilitate disulfide bond rearrangements in mucins indirectly, by recruiting the quality control machinery for the mucin client. It is important to note that the IP/proteomics approach captures both disulfide bonded and non-disulfide bonded AGR2 protein interactions throughout the secretory pathway, whereas the non-reducing western blotting experiments reveal disulfide-bonded interactions with unknown clients. The interaction between AGR2 and MUC5-AC was confirmed in both OE19 esophageal cells (Figure 4) and esophageal adenocarcinoma tissue (Figure 7), with both proteins being co-expressed in the dysplastic mucosa (Figure 8); future pulse-chase experiments will be required to ascertain when and where AGR2-mucin complexes form in esophageal cancer cells, and to establish the temporal nature of these interactions to interrogate the hypothesis that AGR2 acts as a chaperone recruitment scaffold for its main client, MUC-5.

The proteomic analysis of AGR2 complexes revealed some unexpected interactions, for example with BCAP31 and VAPA, which do not have solvent exposed cysteines. VAPA is a tail-anchored protein involved in the biogenesis of autophagosomes (and peroxisomes) from the ER (40). BCAP31 contributes to the transduction of apoptotic signals from the ER to mitochondria during ER stress (22). Thus one possibility could be that the AGR2 interaction with VAPA and/or BCAP31 is indirect and occurs during client enrichment at autophagosome or vesicle recruitment sites. Taken together with the finding that AGR2 interacts with SQSTM1 (Figure 5), another autophagosomal membrane-binding protein, part of

AGR2s function appears to involve working with molecules that determine post-ER compartment fate. Patel et. al. found that proteins involved in autophagosome initiation and elongation were required for effective mucus secretion in colonic goblet cells (26), suggesting that AGR2 interacts with the autophagosomal machinery during mucin granule biogenesis. In strong support of the interactome data (Tables 1 and 2), the Hansson laboratory used an inducible goblet cell line (LS174T) to identify the composition of highly purified mucin-containing vesicles by proteomics. AGR2 and MUC-5AC were identified in these granules along with BiP, ERp29, ERp57, ERp44, ERO1, Prx-IV, SQSTM1, BCAP31, VAPA and aldehyde dehydrogenases (31). Thus the interactions demonstrated in the present paper, including those between AGR2, ALDH3A1 and other metabolic enzymes, could be explained by a fraction of AGR2 interacting with partners in a mucin granule. It is well established that AGR2 has weak ER retention and can be distributed throughout the secretory pathway, consistent with the finding that there is partial colocalisation between AGR2 and ALDH3A1 (Figure 6). Taken together, the immunofluorescence data in this paper support the notion that most, but not all, AGR2 localizes to the ER within OE19 cells (Figure 6). Further analysis will be required (e.g. in an inducible system such as the LS174T cell line) to determine the trafficking and temporal-spatial interaction between AGR2 and mucin granule/autophagosome biogenesis proteins.

The expression of at least some mucins, including MUC-4, can be upregulated by environmental factors (20). It remains possible that AGR2 and MUC-5AC interactions *in vivo* are influenced by the gastrointestinal milieu and it will be worthwhile applying a proteomic approach to tissue models to establish whether longer-term acid reflux in Barrett's esophagus or adenocarcinoma affects the interactome of these proteins *in vivo*. We show that MUC-5AC is overexpressed and co-expressed with AGR2 in Barrett's esophagus and esophageal cancer tissues (Figure 8 and supplementary data), highlighting its dysregulation in gastro-intestinal disease. However, MUC-5AC is also overexpressed and linked to hypersecretion of mucus in chronic obstructive pulmonary disease (15). Thus, the identification of MUC-5AC as a primary client of AGR2 suggests that targeting AGR2 and associated chaperones could also help to control MUC-5AC trafficking and secretion in lung pathologies.

Innovation

This study has identified >20 novel protein interactions to markedly increase the depth of the AGR2 interactome and provide new points of entry to define AGR2 function in health and disease. The results show that pro-oxidants induce the formation of AGR2 complexes. We identify MUC-5 as the principal client of AGR2 in esophageal adenocarcinoma. Identification of an alkylation-sensitive interaction between AGR2 and SQSTM1 directly links AGR2 to oxidative stress responses for the first time. Targeting the AGR2 interactome with anti-oxidants should provide a new avenue for the development of therapies for AGR2 positive cancers and in AGR2 driven lung disease.

Materials and Methods

Chemicals

Fine chemicals were obtained from Sigma-Aldrich/Merck (Dorset, UK) unless otherwise stated. LiChrosolv LC-MS chromatography solvents were from VWR (Leicestershire, UK).

Antibodies

Rabbit monoclonal anti-AGR2 (D9V2F) XP (13062), rabbit polyclonal anti-BiP (3183), rabbit monoclonal anti-ERp44 (D17A6) XP (3798) and rabbit polyclonal anti-SQSTM1 (5114) were purchased from Cell Signalling Technologies (London, UK). Rabbit monoclonal anti-AGR2 (EPR3278/ab76473), mouse monoclonal anti-β-actin (ab8224), rabbit monoclonal anti-MUC-5AC (EPR16904/ab198294), rabbit polyclonal anti-ERp29 (ab11420), mouse monoclonal anti-Prx-IV (7A1) (ab16943) and rabbit polyclonal to alpha-tubulin (ab4074) were purchased from abcam (Cambridge, UK). The mouse monoclonal antibody against AGR2 (6C5; sc-101211) was purchased from Santa Cruz Biotechnology (Dallas, TX, US). Mouse monoclonal anti-PDI RL-90 (MA3-019) was purchased from Thermo Fisher Scientific (Waltham, MA, US). Rabbit anti-ALDH3A1 (15578-1-AP) was purchased from Proteintech (Manchester, UK). The mouse GM130 antibody (610823) was from BD Biosciences (San Jose, CA, US)

Rabbit polyclonal anti-PDI has previously been described (5). Rabbit polyclonal calnexin antibody was a gift from Prof. Masuru Okabe, Osaka University. Secondary antibodies used in western blotting were swine anti-rabbit peroxidase (SARPO P0217) and goat anti-mouse peroxidase (GAMPO P0447) conjugates from DAKO/Agilent (Santa Clara, CA, US). Donkey anti-rabbit and mouse Alexa Fluor 488 and donkey anti-rabbit and mouse Alexa Fluor 594 secondary antibodies were used in immunofluorescence (Thermo Fisher Scientific, Waltham, MA, US).

Antibody dilutions for western blotting were as follows: anti-AGR2 (D9V2F), 1:1000; anti-AGR2 (EPR3278/ab76473) 1:5000; anti-β-actin, 1:10,000; anti-BiP, 1:1000; anti-CNX, 1:2000; anti-ERp29, 1:1000; anti-ERp44, 1:1000; anti-MUC-5AC (ab198294), 1:10,000; anti-PDI pAb, 1:1000; anti-PDI (RL-90), 1:1000; anti-Prx-IV, 1:2000; anti-SQSTM1 1:1000. Secondary antibody dilutions for western blotting were as follows: SARPO, 1:3000; GAMPO 1:3000. Antibody dilutions for immunofluorescence were as follows: anti-alpha tubulin 1 $\mu g\ ml^{-1}$; anti-PDI pAb, 1:200; anti-AGR2 (D9V2F), 1:200; anti-AGR2 (6C5) 1:200; anti-Prx-IV, 1:200; anti-GM130 1:200; anti-ALDH3A1 1:100; anti-MUC-5AC 1:250. Secondary antibody dilutions for immunofluorescence were 1:1000 for: donkey anti-rabbit Alexa Fluor 488, anti-rabbit Alexa Fluor 594, anti-mouse Alexa Fluor 488 and anti-mouse Alexa Fluor 594. Primary antibody dilutions for immunohistochemistry were anti-AGR2 (D9V2F) 1:800, anti-MUC-5AC 1:500, anti-SQSTM1 1:200 and anti-Prx-IV 1:250.

Tissue Culture

The OE19 cell line (JROECL19) was immortalised from an esophageal adenocarcinoma of the cardia designated as pathological stage III (UICC) showing moderate differentiation. The OE33 cell line (JROECL33) was isolated from a lower esophageal Barrett's metaplasia adenocarcinoma designated as pathological stage IIA (UICC) showing poor differentiation (30). The OE19 and OE33 cells were obtained from the ECACC and were subcultured twice weekly at 1:10 in RPMI medium supplemented with 8% fetal bovine serum (Sigma), 2 mM glutamax, 100 units mL^{-1} penicillin, and 100 $\mu g\ mL^{-1}$ streptomycin (all Invitrogen ThermoFisher).

Immunofluorescence and Confocal Microscopy

OE19 cells grown on coverslips were fixed with 4% paraformaldehyde (Agar Scientific, Stansted, UK) in PBS supplemented with 1 mM $CaCl_2$ and 0.5 mM $MgCl_2$ (PBS++) for 10 min. Free aldehyde groups were quenched with 50 mM ammonium chloride in PBS++ for 10 min then the cells were permeabilised with 0.1% Triton X-100 in PBS++ for 10 min. Samples were then blocked in 0.2% BSA in PBS++ twice for 5 min each, then incubated with 25 µL primary antibody solution, diluted 1:200 in 0.2% BSA in PBS++, for either 1 hr at room temperature or overnight at 4 ^{o}C. When using two primary antibodies for co-staining, both were applied simultaneously. Following primary antibody incubation, coverslips were washed three times with PBS++ then incubated with the secondary antibody solution, diluted in 0.2% BSA in PBS++, for 25 min in the dark. Following secondary antibody incubation, coverslips were washed twice with 0.2% BSA in PBS++, twice with PBS++ then incubated with 50 µL of 5 µg/mL DAPI solution for 5 min. Finally, coverslips were rinsed briefly in PBS++ and dH_2O and mounted on microscope slides with vectashield mounting medium (Vectorlabs, Peterborough, UK). Before imaging, slides were left in the dark at 4°C overnight to allow the vectashield to set. The slides were imaged on a confocal microscope (Zeiss 880).

Cell Treatments with Diamide

Stock solids of the chemical diamide (N,N,N',N'-Tetramethylazodicarboxamide) were dissolved in dH_2O and used fresh, or aliquoted and frozen at -20°C prior to treatment. Cells in 6 cm dishes were treated with fresh RPMI media supplemented with 5 mM diamide and returned to the 37°C incubator for the required time course. Following treatment cells were washed twice with PBS. The PBS wash was supplemented with 20 mM NEM in experiments that required alkylation of free protein –SH groups. Cells were lysed immediately after treatment.

Cell and Tissue Lysis

Cells were lysed on ice in 300 µL of MNT lysis buffer (20 mM 4- morpholineethanesulfonic acid, 30 mM Tris, 100 mM NaCl, pH 7.4) with 1% Triton X- 100, supplemented with 10 µg mL^{-1} each of the protease inhibitors chymostatin, leupeptin, antipain, and pepstatin A. Lysis buffer also contained 20 mM NEM in the alkylation experiments. Tissues were lysed in the same buffers and homogenised by mechanical disruption prior to analysis. The lysates were dispensed into Eppendorf tubes and vortexed. The cell nuclei were removed by centrifugation at 16,100 xg (Eppendorf microcentrifuge) for 10 min at 4°C and the supernatants were collected in fresh Eppendorf tubes, flash frozen in liquid nitrogen and stored at -20°C; or used immediately for gel analysis.

Protein Determination

Protein concentrations were determined using the Bio-Rad Protein Assay procedure with BSA used as a standard (Bio-Rad, Hercules, CA, US). Standards were created by combining the Bradford dye with dH_2O, 0.1 M HCl, 1 mg mL^{-1} BSA and lysis buffer. For samples, the Bradford dye was mixed with dH_2O, 0.1 M HCl, lysis buffer and 2 µL of lysate. Mixtures were left for 10 min, then vortexed and the absorbance measured at 595 nm with an Eppendorf Biophotometer.

SDS-PAGE

Both reducing and non-reducing conditions were used to analyse proteins by SDS-PAGE. Samples were prepared by adding 2x Laemmli sample buffer (4% SDS, 20% glycerol, 0.004% bromophenol blue and 0.125 M Tris HCl +/- 50 mM DTT). Samples were heated at 95 °C for 5 min, centrifuged at 16,100 xg for 5 min, then analysed using either 8 %, 10 % or 12 % polyacrylamide gels (Hoefer, Holliston, MA, US). The resolving gel was comprised of: 0.375 M Tris (pH 8.8), 0.1% SDS, 0.1% APS and 0.04% TEMED. The stacking gel was comprised of: 5% acrylamide, 0.125 M Tris (pH 6.8), 0.1% SDS, 0.075% APS, 0.1% TEMED. Samples were loaded alongside a precision plus protein marker (Bio-Rad). Gels were run at 10-50 mA for approximately 1 hr in a Hoefer mighty small II mini vertical

electrophoresis unit containing 1x Tris-glycine running buffer (25 mM Tris, 192 mM glycine, 0.1% SDS, pH 8.3).

Western Blotting

Proteins were transferred to PVDF membranes after SDS-PAGE separation. The membranes were first submerged in methanol for 20 seconds, then briefly wetted in transfer buffer (25 mM Tris base, 190 mM glycine and 20% methanol in dH_2O). Proteins were transferred to the membranes from the SDS-PAGE gel at either 150 mA for 2 hrs or at 30 V overnight. Membranes were then blocked in 5% non-fat dry milk in TBS-T (Tris-buffered saline (10 mM Tris base, 70 mM NaCl, 1.34 mM KCl) containing 0.1% Tween 20) for 1 hr at room temperature. Membranes were washed 5 times with TBS-T before either a 1 hr incubation at room temperature or an overnight incubation at 4°C with primary antibody (dependent on antibody). The primary antibody incubation was followed by another 5 washes with TBS-T and incubation for 1 hr at room temperature with either SARPO or GAMPO secondary antibodies (DAKO/Agilent). To visualise protein localisation, 500 µL of ECL solution per membrane was used (GE Healthcare, Chicago, IL, US). Membranes were exposed to photographic light sensitive film (Kodak, Rochester, NY, US) in a dark room and subsequently developed in an X-ray developer machine (XOMAT). Western blot semi-quantification by densitometry was performed on scanned immunoblot images with the ImageJ image processing program. Western blotting experiments were repeated at least twice and unedited full-length blots accompany the manuscript as supplementary Figures.

Immunoprecipitation

Immunoprecipitation of proteins was performed using Protein A-Sepharose beads (Sigma). Protein A-Sepharose beads (10% w/v packed beads) were washed in lysis buffer and incubated with the indicated primary antibodies for 1 hr at 4°C followed by three washes with lysis buffer (20 mM 4-morpholineethanesulfonic acid, 30 mM Tris, 100 mM NaCl, pH 7.4) containing 1% Triton X-100. The bead-antibody mixture was then incubated with 200 µL cell lysate overnight at 4°C and washed with lysis

buffer another five times, keeping an aliquot of the lysate supernatant for western blotting analysis. The final wash was performed without 1% Triton X-100 when preparing samples for mass spectrometry. Negative controls for mass spectrometry were prepared by incubating Protein A-sepharose beads with lysates. Samples were eluted using either 50 µL of 2x Laemmli sample buffer if intended for western blotting or 30 µL elution buffer (4% SDS, 100 mM DTT, 100 mM Tris-HCl) if intended for mass spectrometry.

Proteomics and Mass Spectrometry

Eluted immunoprecipitated samples or cell lysates were trypsin digested using a FASP Kit (44250; Expedeon, San Diego, CA, US). Of the 30 µL of elute sample produced from an IP, 2 µL was used in a Bradford protein determination assay. FASP digestion was performed by adding 28 µL of protein extract to a spin filter followed by washing in urea to reduce the concentration of SDS in the filter. Samples were then alkylated with 0.05M iodoacetamide and transferred into ammonium bicarbonate by buffer exchanges on the spin-filter before enzymatic digestion with trypsin (Trypsin Gold, Promega, Southampton, UK) at a 1:100 enzyme-to-protein ratio for 16 hr. Recovered peptides were acidified with TFA and analysed by data-dependent LC-MS/MS on a TripleTOF 6600 mass spectrometer (Sciex, Warrington, UK) linked to an Eksigent 425 liquid chromatography system via a Sciex nanospray III source. Final FASP eluates were freeze-dried and the residue re-suspended at 1 µg μL^{-1} in 2% acetonitrile, 0.1% formic acid for LC-MS injection. Nanoflow chromatographic separation of peptides used a trap-and-elute method with an Acquity M-class Symmetry C18 Trap column, 100Å, 5 µm, 180 µm x 20 mm (Waters, Milford, MA, US), and a PicoFrit packed emitter column 75 µm x 250 mm with a 10 µm tip containing 3 µm Reprosil-PUR silica (New Objective, Woburn, MA, US). One microgram of peptide samples were transferred onto the trap column within a 25 µL volume of 0.1% formic acid at 5 µL min^{-1} before injection valve switching and running of a gradient at 300 nL min^{-1}. Buffer A was composed of 0.1% formic acid in water, buffer B was composed of 0.1% formic acid in acetonitrile. Sequential linear gradients of 1 to 28% B over 50 min and 28 to 80% B over 5 min were followed by a 5 min column wash

in 80% B. Return to 1% B was performed over 3 min and the column was then re-equilibrated in this buffer for 27 min. Data-dependent top-30 MS-MS acquisition was started immediately upon gradient initiation and was for 80 min. Throughout this period, precursor-ion scans (400 to 1600 m/z) of 250 ms enabled selection of up to 30 multiply-charged ions for CID fragmentation and MS/MS spectrum acquisition (m/z 100-1600) for 33 ms. Rolling precursor exclusion of 15 sec was applied to limit multiple fragmentation of the same peptide. Precursor and fragment-ion lists in mgf format were generated from wiff format raw MS data-files using MSConvert (ProteoWizard software suite). Protein identification used the database search engine Mascot 2.5.1. and a database containing Uniprot human db download (6-4-17) plus 9 protease/GFP/YFP sequences. The peptide false discovery rate from a target decoy database was set at ≤1% and a filter of >1 unique peptide sequence per protein applied. Protein identifications based on a non-unique peptide were also excluded from further analysis. Data were further processed in ProteinPilot to obtain peptide lists and calculate percentage coverage of identified proteins.

Immunohistochemistry and Tissues

Anonymised tissue sections obtained from the archives at James Cook University Hospital, Middlesbrough, UK and fresh esophageal/adenocarcinoma tissue was classified by an experienced gastrointestinal pathologist at the time of biopsy. Tissue usage was approved by the NHS research ethics committee, references 05/Q1003/36 and 09/H0908/24. Tissue sections (4 microns) were either stained by an automated system using the Ventana Ultraview DAB detection system (Roche Diagnostics, Basel, Switzerland) or processed manually. For manual staining, tissue sections embedded in paraffin were incubated at 50 °C overnight prior to staining. Sections were deparaffinised with two 7 min washes in Histoclear (National Diagnostics, Atlanta, GA, US), one 7 min wash in 100% ethanol, one 5 min wash in 95% ethanol and one 5 min wash in 70% ethanol. Sections were then hydrated in dH_2O for 3 min. Antigen retrieval was achieved by treating the sections with 3% H_2O_2 in MeOH for 15 min followed by 20 min in 10 mM Na-citrate (pH 6.0) at 90 °C. Slides were cooled on ice, followed by a 5 min wash in 0.2% BSA in PBS and a 30 min blocking incubation in 0.2% BSA + 5% normal goat serum (DAKO, X0907) in PBS.

Sections were then incubated with antibodies diluted in PBS + 0.2% BSA + 2% normal goat serum for 1 hr. After primary incubation, sections were washed in 0.2% BSA in PBS for 5 min, followed by a 45 min incubation with the secondary antibody goat anti-mouse/rabbit biotin (made by mixing 2 mL PBS with 20 µL reagent C from the Dako/Agilent kit, K0492). Slides were washed in 0.2% BSA in PBS for 5 min and then incubated with a reagent A/B mixture (made by mixing 2 mL PBS with 20 µL reagent A and 20 µL reagent B) for 30 min. DAB solution was applied to the sections and they were allowed to develop for ~5 min before submersion in dH_2O to stop the reaction. Slides were then counter-stained with haematoxylin for 4 min, followed by rinsing in dH_2O, 1% HCl in MeOH, dH_2O, tap water, 70% EtOH, 95% EtOH, a 5 min wash in 100% EtOH, two 7 min washes in Histoclear and finally mounted in DPX (Agar Scientific, R1340). Immunohistochemical experiments were performed three times using material from 3 independent blocks for each tissue type and representative slides were imaged with a Leica ICC50 microscope.

Alcian Blue Staining

Alcian Blue was used as a stain for acid-simple mucins (including MUC-5AC/B). Tissue sections embedded in paraffin were incubated at 50 °C overnight prior to staining. Sections were deparaffinised and hydrated as described above, washed in 3% acetic acid for 3 min then stained with a pH 2.5, 0.5% Alcian Blue solution in 2% aqueous acetic acid for 30 min. Following staining, sections were rinsed in tap water for 10 min and then rinsed briefly in dH_2O. Slides were then co-stained with haematoxylin for 6 min, then subsequently rinsed in dH_2O, 1% HCl in MeOH, dH_2O, tap water, 70% EtOH, 95% EtOH, a 5 min wash in 100% EtOH, two 7 min washes in Histoclear and finally mounting in DPX (Agar Scientific, R1340).

Acknowledgements

We thank Joanne Robson and Tim Hawkins for guidance on confocal microscopy; Eve Hunter-Featherstone, Matthew Freer and Iakowos Karakesisoglou for antibody and IHC advice; and Graeme

Watson, Anjan Dhar and Janusz Jankowski for helpful suggestions and discussions. We thank the Esophageal Cancer Support Group, James Cook University Hospital, Middlesbrough, UK, for contributing funding for this project. The authors declare that they have no conflicts of interest with the contents of this article.

List Of Abbreviations

The abbreviations used are: ADAM, A disintegrin and metalloprotease; ALDH, aldehyde dehydrogenase; APS, ammonium persulfate; AREG, amphiregulin; AGR, anterior gradient; BCAP, B-cell adapter for phosphoinositide 3-kinase; BiP, binding protein; BSA, bovine serum albumin; CID, collision-induced dissociation; DAB, 3,3'-diaminobenzidine, DAPI, 4',6-Diamidine-2'-phenylindole dihydrochloride; DPX, distrene-plasticizer-xylene; ECL, enhanced chemiluminescence; ER, endoplasmic reticulum; EGFR, epidermal growth factor receptor; ERO, endoplasmic reticulum oxidoreductase; ESI, electrospray ionisation; FASP, filter aided sample preparation; GAMPO, goat anti-mouse peroxidase; GFP, green fluorescent protein; GO, gene ontology; GRP, glucose regulated protein; Hsp, heat shock protein; IP, immunoprecipitation; KEAP, Kelch-like ECH-associated protein; LC-MS, liquid chromatography–mass spectrometry; MUC, mucin; NEM, N-ethylmaleimide; NMR, nuclear magnetic resonance; OE, esophageal; OG, esophageal-gastric; PBS, phosphate buffered saline; PDI, Protein Disulfide Isomerase; PDILT, PDI-like protein of the testis; Prx-IV, peroxiredoxin IV; PTGR1, prostaglandin reductase 1; PVDF, polyvinylidene fluoride; RPMI, Roswell Park Memorial Institute; SARPO, swine anti-rabbit peroxidase; TAGLN, transgelin; TEMED, tetramethylethylenediamine; TFA, trifluoroacetic acid; TGF, transforming growth factor; TOF, time-of-flight; YFP, yellow fluorescent protein.

References

1. Aberger F, Weidinger G, Grunz H, and Richter K. Anterior specification of embryonic ectoderm: the role of the Xenopus cement gland-specific gene XAG-2. *Mech Dev* 72: 115–130, 1998.
2. Adler KB, Tuvim MJ, and Dickey BF. Regulated Mucin Secretion from Airway Epithelial Cells. *Front Endocrinol (Lausanne)* 4, 2013.
3. Antoniou AN and Powis SJ. Characterization of the ERp57-Tapasin Complex by Rapid Cellular Acidification and Thiol Modification. *Antioxidants & Redox Signaling* 5: 375–379, 2003.
4. Battle DM, Gunasekara SD, Watson GR, Ahmed EM, Saysell CG, Altaf N, Sanusi AL, Munipalle PC, Scoones D, Walker J, Viswanath Y, and Benham AM. Expression of the Endoplasmic Reticulum Oxidoreductase Ero1α in Gastro-Intestinal Cancer Reveals a Link Between Homocysteine and Oxidative Protein Folding. *Antioxidants & Redox Signaling* 19: 24–35, 2013.
5. Benham AM, Cabibbo A, Fassio A, Bulleid N, Sitia R, and Braakman I. The CXXCXXC motif determines the folding, structure and stability of human Ero1 - Lα. *The EMBO Journal* 19: 4493–4502, 2000.
6. Block KI, Gyllenhaal C, Lowe L, Amedei A, Amin ARMR, Amin A, Aquilano K, Arbiser J, Arreola A, Arzumanyan A, Ashraf SS, Azmi AS, Benencia F, Bhakta D, Bilsland A, Bishayee A, Blain SW, Block PB, Boosani CS, Carey TE, Carnero A, Carotenuto M, Casey SC, Chakrabarti M, Chaturvedi R, Chen GZ, Chen H, Chen S, Chen YC, Choi BK, Ciriolo MR, Coley HM, Collins AR, Connell M, Crawford S, Curran CS, Dabrosin C, Damia G, Dasgupta S, DeBerardinis RJ, Decker WK, Dhawan P, Diehl AME, Dong J-T, Dou QP, Drew JE, Elkord E, El-Rayes B, Feitelson MA, Felsher DW, Ferguson LR, Fimognari C, Firestone GL, Frezza C, Fujii H, Fuster MM, Generali D, Georgakilas AG, Gieseler F, Gilbertson M, Green MF, Grue B, Guha G, Halicka D, Helferich WG, Heneberg P, Hentosh P, Hirschey MD, Hofseth LJ, Holcombe RF, Honoki K, Hsu H-Y, Huang GS, Jensen LD, Jiang WG, Jones LW, Karpowicz PA, Keith WN, Kerkar SP, Khan GN, Khatami M, Ko YH, Kucuk O, Kulathinal RJ, Kumar NB, Kwon BS, Le A, Lea MA, Lee H-Y, Lichtor T, Lin L-T, Locasale JW, Lokeshwar BL, Longo VD, Lyssiotis CA, MacKenzie KL, Malhotra M, Marino M, Martinez-

Chantar ML, Matheu A, Maxwell C, McDonnell E, Meeker AK, Mehrmohamadi M, Mehta K, Michelotti GA, Mohammad RM, Mohammed SI, Morre DJ, Muralidhar V, Muqbil I, Murphy MP, Nagaraju GP, Nahta R, Niccolai E, Nowsheen S, Panis C, Pantano F, Parslow VR, Pawelec G, Pedersen PL, Poore B, Poudyal D, Prakash S, Prince M, Raffaghello L, Rathmell JC, Rathmell WK, Ray SK, Reichrath J, Rezazadeh S, Ribatti D, Ricciardiello L, Robey RB, Rodier F, Rupasinghe HPV, Russo GL, Ryan EP, Samadi AK, Sanchez-Garcia I, Sanders AJ, Santini D, Sarkar M, Sasada T, Saxena NK, Shackelford RE, Shantha Kumara HMC, Sharma D, Shin DM, Sidransky D, Siegelin MD, Signori E, Singh N, Sivanand S, Sliva D, Smythe C, Spagnuolo C, Stafforini DM, Stagg J, Subbarayan PR, Sundin T, Talib WH, Thompson SK, Tran PT, Ungefroren H, Vander Heiden MG, Venkateswaran V, Vinay DS, Vlachostergios PJ, Wang Z, Wellen KE, Whelan RL, Yang ES, Yang H, Yang X, Yaswen P, Yedjou C, Yin X, Zhu J, and Zollo M. Designing a broad-spectrum integrative approach for cancer prevention and treatment. *Seminars in Cancer Biology* 35: S276–S304, 2015.

7. Carroll B, Otten EG, Manni D, Stefanatos R, Menzies FM, Smith GR, Jurk D, Kenneth N, Wilkinson S, Passos JF, Attems J, Veal EA, Teyssou E, Seilhean D, Millecamps S, Eskelinen E-L, Bronowska AK, Rubinsztein DC, Sanz A, and Korolchuk VI. Oxidation of SQSTM1/p62 mediates the link between redox state and protein homeostasis. *Nature Communications* 9: 256, 2018.
8. Dong A, Gupta A, Pai RK, Tun M, and Lowe AW. The human adenocarcinoma-associated gene, AGR2, induces expression of amphiregulin through Hippo pathway co-activator YAP1 activation. *J Biol Chem* 286: 18301–18310, 2011.
9. Fessart D, Domblides C, Avril T, Eriksson LA, Begueret H, Pineau R, Malrieux C, Dugot-Senant N, Lucchesi C, Chevet E, and Delom F. Secretion of protein disulphide isomerase AGR2 confers tumorigenic properties. *Elife* 5, 2016.
10. Fujimoto T, Nakamura O, Saito M, Tsuru A, Matsumoto M, Kohno K, Inaba K, and Kadokura H. Identification of the physiological substrates of PDIp, a pancreas-specific protein-disulfide isomerase family member. *J Biol Chem* 293: 18421–18433, 2018.

11. Gupta A, Dong A, and Lowe AW. AGR2 gene function requires a unique endoplasmic reticulum localization motif. *J Biol Chem* 287: 4773–4782, 2012.

12. Higa A, Mulot A, Delom F, Bouchecareilh M, Nguyên DT, Boismenu D, Wise MJ, and Chevet E. Role of pro-oncogenic protein disulfide isomerase (PDI) family member anterior gradient 2 (AGR2) in the control of endoplasmic reticulum homeostasis. *J Biol Chem* 286: 44855–44868, 2011.

13. Jessop CE, Chakravarthi S, Garbi N, Hämmerling GJ, Lovell S, and Bulleid NJ. ERp57 is essential for efficient folding of glycoproteins sharing common structural domains. *EMBO J* 26: 28–40, 2007.

14. Jessop CE, Watkins RH, Simmons JJ, Tasab M, and Bulleid NJ. Protein disulphide isomerase family members show distinct substrate specificity: P5 is targeted to BiP client proteins. *Journal of Cell Science* 122: 4287–4295, 2009.

15. Kesimer M, Ford AA, Ceppe A, Radicioni G, Cao R, Davis CW, Doerschuk CM, Alexis NE, Anderson WH, Henderson AG, Barr RG, Bleecker ER, Christenson SA, Cooper CB, Han MK, Hansel NN, Hastie AT, Hoffman EA, Kanner RE, Martinez F, Paine R, Woodruff PG, O'Neal WK, and Boucher RC. Airway Mucin Concentration as a Marker of Chronic Bronchitis. *New England Journal of Medicine* 377: 911–922, 2017.

16. Komatsu M, Kurokawa H, Waguri S, Taguchi K, Kobayashi A, Ichimura Y, Sou Y-S, Ueno I, Sakamoto A, Tong KI, Kim M, Nishito Y, Iemura S, Natsume T, Ueno T, Kominami E, Motohashi H, Tanaka K, and Yamamoto M. The selective autophagy substrate p62 activates the stress responsive transcription factor Nrf2 through inactivation of Keap1. *Nature Cell Biology* 12: 213, 2010.

17. Komiya T and Tanigawa Y. Cloning of the gene gob-4, which is expressed in intestinal goblet cells in mice. *BBA* 1444: 434–438, 1999.

18. Kosower NS, Kosower EM, Wertheim B, and Correa WS. Diamide, a new reagent for the intracellular oxidation of glutathione to the disulfide. *Biochem Biophys Res Commun* 37: 593–596, 1969.

19. Liu D, Rudland PS, Sibson DR, Platt-Higgins A, and Barraclough R. Human homologue of cement gland protein, a novel metastasis inducer associated with breast carcinomas. *Cancer Res* 65: 3796–3805, 2005.

20. Mariette C, Perrais M, Leteurtre E, Jonckheere N, Hémon B, Pigny P, Batra S, Aubert J-P, Triboulet J-P, and Seuningen IV. Transcriptional regulation of human mucin MUC4 by bile acids in oesophageal cancer cells is promoter-dependent and involves activation of the phosphatidylinositol 3-kinase signalling pathway. *Biochemical Journal* 377: 701–708, 2004.

21. Mohtar MA, Hernychova L, O'Neill JR, Lawrence ML, Murray E, Vojtesek B, and Hupp TR. The Sequence-specific Peptide-binding Activity of the Protein Sulfide Isomerase AGR2 Directs Its Stable Binding to the Oncogenic Receptor EpCAM. *Mol Cell Proteomics* 17: 737–763, 2018.

22. Namba T, Tian F, Chu K, Hwang S-Y, Yoon KW, Byun S, Hiraki M, Mandinova A, and Lee SW. CDIP1-BAP31 Complex Transduces Apoptotic Signals from Endoplasmic Reticulum to Mitochondria under Endoplasmic Reticulum Stress. *Cell Reports* 5: 331–339, 2013.

23. Pankiv S, Clausen TH, Lamark T, Brech A, Bruun J-A, Outzen H, Øvervatn A, Bjørkøy G, and Johansen T. p62/SQSTM1 Binds Directly to Atg8/LC3 to Facilitate Degradation of Ubiquitinated Protein Aggregates by Autophagy. *J Biol Chem* 282: 24131–24145, 2007.

24. Park K, Chung YJ, So H, Kim K, Park J, Oh M, Jo M, Choi K, Lee E-J, Choi Y-L, Song SY, Bae D-S, Kim B-G, and Lee J-H. AGR2, a mucinous ovarian cancer marker, promotes cell proliferation and migration. *Exp Mol Med* 43: 91–100, 2011.

25. Park S-W, Zhen G, Verhaeghe C, Nakagami Y, Nguyenvu LT, Barczak AJ, Killeen N, and Erle DJ. The protein disulfide isomerase AGR2 is essential for production of intestinal mucus. *Proc Natl Acad Sci U S A* 106: 6950–6955, 2009.

26. Patel KK, Miyoshi H, Beatty WL, Head RD, Malvin NP, Cadwell K, Guan J, Saitoh T, Akira S, Seglen PO, Dinauer MC, Virgin HW, and Stappenbeck TS. Autophagy proteins control goblet cell function by potentiating reactive oxygen species production. *EMBO J* 32: 3130, 2013.

27. Patel P, Clarke C, Barraclough DL, Jowitt TA, Rudland PS, Barraclough R, and Lian L-Y. Metastasis-promoting anterior gradient 2 protein has a dimeric thioredoxin fold structure and a role in cell adhesion. *J Mol Biol* 425: 929–943, 2013.

28. Pohler E, Craig AL, Cotton J, Lawrie L, Dillon JF, Ross P, Kernohan N, and Hupp TR. The Barrett's antigen anterior gradient-2 silences the p53 transcriptional response to DNA damage. *Mol Cell Proteomics* 3: 534–547, 2004.

29. Ramachandran V, Arumugam T, Wang H, and Logsdon CD. Anterior gradient 2 is expressed and secreted during the development of pancreatic cancer and promotes cancer cell survival. *Cancer Res* 68: 7811–7818, 2008.

30. Rockett JC, Larkin K, Darnton SJ, Morris AG, and Matthews HR. Five newly established oesophageal carcinoma cell lines: phenotypic and immunological characterization. *Br J Cancer* 75: 258–263, 1997.

31. Rodríguez-Piñeiro AM, Post S van der, Johansson MEV, Thomsson KA, Nesvizhskii AI, and Hansson GC. Proteomic Study of the Mucin Granulae in an Intestinal Goblet Cell Model. *J Proteome Res* 11: 1879–1890, 2012.

32. Ryu J, Park SG, Lee PY, Cho S, Lee DH, Kim GH, Kim J-H, and Park BC. Dimerization of pro-oncogenic protein Anterior Gradient 2 is required for the interaction with BiP/GRP78. *Biochem Biophys Res Commun* 430: 610–615, 2013.

33. Schroeder BW, Verhaeghe C, Park S-W, Nguyenvu LT, Huang X, Zhen G, and Erle DJ. AGR2 Is Induced in Asthma and Promotes Allergen-Induced Mucin Overproduction. *Am J Respir Cell Mol Biol* 47: 178–185, 2012.

34. Sommerova L, Ondrouskova E, Vojtesek B, and Hrstka R. Suppression of AGR2 in a TGF-β-induced Smad regulatory pathway mediates epithelial-mesenchymal transition. *BMC Cancer* 17: 546, 2017.

35. Thompson DA and Weigel RJ. hAG-2, the human homologue of the Xenopus laevis cement gland gene XAG-2, is coexpressed with estrogen receptor in breast cancer cell lines. *Biochem Biophys Res Commun* 251: 111–116, 1998.

36. Tokuhiro K, Ikawa M, Benham AM, and Okabe M. Protein disulfide isomerase homolog PDILT is required for quality control of sperm membrane protein ADAM3 and male fertility. *Proc Natl Acad Sci USA* 109: 3850, 2012.

37. Tomoshige K, Guo M, Tsuchiya T, Fukazawa T, Fink-Baldauf IM, Stuart WD, Naomoto Y, Nagayasu T, and Maeda Y. An EGFR ligand promotes EGFR -mutant but not KRAS -mutant lung cancer in vivo. *Oncogene* 37: 3894–3908, 2018.

38. Zhang J-S, Gong A, Cheville JC, Smith DI, and Young CYF. AGR2, an androgen-inducible secretory protein overexpressed in prostate cancer. *Genes Chromosomes Cancer* 43: 249–259, 2005.

39. Zhao F, Edwards R, Dizon D, Mastroianni JR, Geyfman M, Ouellette AJ, Andersen B, and Lipkin SM. Disruption of Paneth and goblet cell homeostasis and increased endoplasmic reticulum stress in Agr2−/− mice. *Dev Biol* 338: 270–279, 2010.

40. Zhao YG, Liu N, Miao G, Chen Y, Zhao H, and Zhang H. The ER Contact Proteins VAPA/B Interact with Multiple Autophagy Proteins to Modulate Autophagosome Biogenesis. *Current Biology* 28: 1234-1245.e4, 2018.

41. Zhu H, Lam DCL, Han KC, Tin VPC, Suen WS, Wang E, Lam WK, Cai WW, Chung LP, and Wong MP. High resolution analysis of genomic aberrations by metaphase and array comparative genomic hybridization identifies candidate tumour genes in lung cancer cell lines. *Cancer Lett* 245: 303–314, 2007.

Tables

Table 1: Major proteins identified by IP and mass spectrometry that interact with AGR2 in OE19 cells (no diamide). Cov = coverage.

Gene Name	Peptides (95%)	%Cov	%Cov (50)	%Cov (95)	GO function
MUC5AC	29	17.6	17.4	12.4	ECM constituent
AGR2	27	61.7	46.9	41.1	mucus secretion
GRP78	22	40.1	39.0	39.0	chaperone
ALDH3A1	13	31.1	29.6	27.6	metabolism
MUC5B	11	8.5	7.7	7.2	ECM constituent
YWHAZ	8	37.1	37.1	30.2	membrane organisation;
TAGLN2	3	22.1	16.6	16.6	epithelial cell differentiation
ANXA2	3	18.3	11.8	9.2	ECM constituent; exocytosis
S100A6	2	27.8	16.7	16.7	calcium binding; signal transduction
S100P	2	24.2	24.2	24.2	calcium binding; proliferation
PDIA3	2	12.5	12.5	4.8	disulfide oxidoreductase
CANX	2	4.9	4.9	3.5	calcium binding; protein folding

Table 2: Major proteins identified by IP and mass spectrometry that interact with AGR2 in OE19 cells (with diamide). Proteins highlighted in bold were not detectable in the absence of diamide. Cov = coverage.

Gene Name	Peptides (95%)	%Cov	%Cov (50)	%Cov (95)	GO function
MUC5B	76	35.3	33.1	27.9	ECM constituent
MUC5AC	57	27.1	26.0	22.8	ECM constituent
AGR2	50	65.1	65.1	65.1	mucus secretion
GRP78	31	49.9	49.9	47.1	ER chaperone
ALDH3A1	12	35.5	32.7	30.9	metabolism
ERp29	9	43.7	43.7	40.6	ER chaperone
YWHAZ	9	57.6	53.5	39.6	membrane organisation
PRX-IV	7	41.7	39.5	36.9	redox; oxidative stress
ANXA2	6	38.4	36.0	23.3	ECM constituent; exocytosis
ERO1A	4	17.3	13.7	10.5	disulfide oxidoreductase
PDIA3	4	18.6	18.6	8.5	protein disulfide isomerase
TAGLN2	3	24.1	24.1	18.6	epithelial cell differentiation
VAPA	2	30.5	25.3	10.4	vesicle transport
PTGR1	2	18.5	14.3	8.8	oxidoreductase
BCAP31	2	11.8	11.8	8.1	ER degradation; cargo receptor
ERp44	2	11.6	8.1	8.1	protein disulfide isomerase
PDIA6	2	8.0	5.9	5.9	protein disulfide isomerase
CANX	2	6.1	6.1	3.5	calcium binding; protein folding

Table 3: Mucins detected by mass spectrometry of OE19 and OE33 cell lysates. Cov = coverage.

OE19					**OE33**				
Protein	**Peptides (95%)**	**%Cov**	**%Cov (50)**	**%Cov (95)**	**Protein**	**Peptides (95%)**	**%Cov**	**%Cov (50)**	**%Cov (95)**
MUC1	8	50.7	50.3	47.5	MUC20	1	5.2	5.2	2.4
MUC5	7	2.6	2.5	2.1					
MUC12	1	1.22	1.02	1.0					
MUC13	3	6.8	6.8	6.8					

Table 4: Proteins identified by IP and mass spectrometry that interact with ALDH3A1 in OE19 cells. Cov = coverage.

Gene Name	**Peptides (95%)**	**%Cov**	**%Cov (50)**	**%Cov (95)**	**GO Function**
ALDH3A1	5	15.9	11.9	10.4	dehydrogenase
PRDX1	4	32.7	32.7	20.1	redox
ANXA2	3	17.4	11.8	9.1	peroxiredoxin
CASP14	3	17.8	17.8	14.5	calcium binding
CSTA	3	50	50	42.9	protease inhibitor
LCN1	2	19.9	19.9	12.5	ligand binding
DCD	2	40.9	20	20	antimicrobial
TXN	2	20.9	20.9	20.9	redox
PIP	2	17.8	17.8	17.8	glucose transport
AGR2	2	10.3	10.3	10.3	mucus secretion

Table 5: Proteins identified by IP and mass spectrometry that interact with AGR2 in OE19 cells (with no NEM). Proteins highlighted in bold were not detectable in the presence of NEM. Cov = coverage.

Gene Name	**Peptides (95%)**	**%Cov**	**%Cov(50)**	**%Cov(95)**	**GO function**
AGR2	23	55.4	55.4	44.6	mucus secretion
SQSTM	3	21.4	18.1	9.1	autophagy
PKM	2	12.7	10.7	4.2	glycolysis
MUC5B	2	4.2	2.4	1.3	ECM constituent
APOD	2	13.5	10.2	10.2	lipid binding
AKR1C3	2	6.3	6.3	6.3	aldoketo reductase

Table 6: Proteins IPed with the AGR2 antibody from AGR2^{low} OE33 cell lysates (with no NEM). Proteins highlighted in bold were also detected in OE19 cell lysate IPs. Cov = coverage.

Gene Name	Peptides (95%)	%Cov	%Cov (50)	%Cov (95)	GO Function
AGR2	14	49.1	38.9	34.3	mucus secretion
ENOA	7	32	26.7	16.4	glycolysis
PKM	6	24.5	16	14	glycolysis
S100A9	6	33.3	33.3	32.5	calcium binding; proliferation
LDHB	5	25.5	20.4	17.7	metabolism
LDHA	5	23.2	17.2	14.5	metabolism
S100A7	3	36.6	36.6	23.8	calcium binding; proliferation
FASN	3	3.9	2.4	1.2	fatty acid synthesis
XRCC5	3	4.29	4.2	4.2	DNA repair
GPI	3	7.89	7.8	7.8	glycolysis
S100A8	2	28	28	19.3	calcium binding; proliferation
AHCY	2	9.3	7.2	5.3	metabolism
PRDX6	2	16.1	9.4	9.4	peroxidase
ATP5B	2	16	6.1	6.1	ATP synthesis
TCP1	2	9.3	6	6	cytosolic chaperone
RAB15	2	10.4	10.4	10.38	GTPase

Figure legends

Figure 1: AGR2 is expressed in OE19 cells but not in OE33 cells.
OE19 and OE33 cell lysates were analysed by SDS-PAGE and reducing western blotting with antibodies against ER chaperones AGR2 (D9V2F), Prx-IV, ERp29, PDI and calnexin (CNX). β-actin was used as a loading control. One representative experiment is shown (N=3). Full length unedited blots are provided as supplementary data.

Figure 2: Diamide induces disulfide dependent AGR2 complex formation.
(A) Schematic demonstrating alkylation of cysteine residues and trapping of AGR2 interacting proteins (clients) with NEM. Note that AGR2 only has one free cysteine at C81. (B) OE19 cells were treated with 5 mM diamide for 0, 5 or 10 min, followed by lysis and western blotting analysis with the D9V2F AGR2 mAb under reducing and non-reducing conditions. AGR2 complexes appeared in diamide treated lanes under non-reducing conditions (lanes 4-6). (C) β-actin blotting control. (D) OE19 cells were treated with diamide for 0 min (lanes 1 and 6) or 5 min (lanes 2 and 7), washed and allowed to recover (r) for 5, 10 and 20 min (lanes 3,4,5,8,9,10) prior to alkylation, lysis and western blotting for AGR2 under reducing (lanes 1-5) and non-reducing (lanes 6-10) conditions. Upon recovery (lanes 8-10) most complexes persist, however some declined (e.g. *). (E) β-actin blotting control. kDa markers are shown on the left; dia = diamide. One representative experiment is shown (N=3). Full length unedited blots of (C) and (E) are provided as supplementary data.

Figure 3: IP of AGR2 from OE19 cells.
OE19 cells were treated with 5 mM diamide, alkylated, lysed and IPed with the AGR2 mAb (ab76473) and immunoblotted with the AGR2 mAb D9V2F. AGR2 was specifically retrieved in both the presence and absence of diamide (dia; lanes 4 and 5). One representative experiment is shown (N=3). kDa markers are shown on the left. The full length unedited blot is provided as supplementary data.

Figure 4: AGR2 interacts with MUC-5AC, BiP/GRP78, ERp44 and Prx-IV.
OE19 lysates from cells treated +/- diamide (dia) were IPed with the AGR2 mAb ab76473 followed by 8% SDS-PAGE and western blotting analysis for the protein of interest under reducing conditions. (A) AGR2 IP probed with the MUC-5AC mAb EPR16904 showed that AGR2 interacted with MUC-5AC (lanes 2-3) but not IgG alone (lane 1). (B) AGR2 interacted with BiP (upper panel), ERp44 (middle panel) and Prx-IV (lower panel) after diamide treatment (lane 3). (C) Lysate inputs prior to IP were immunoblotted for BiP, ERp44 and Prx-IV and showed similar protein amounts. One representative

experiment is shown (N=2). kDa markers are shown on the left. Full length unedited blots of (B) and (C) are provided as supplementary data.

Figure 5: AGR2 interacts with SQSTM1 in OE19 cells

(A) Lysates from OE19 cells and OE33 cells were analysed for the expression of SQSTM1 by western blotting (lanes 1 and 2) or were subjected to IP with the AGR2 antibody ab76473 prior to western blotting for SQSTM1 (lanes 3 and 4). SQSTM1 co-IPed with AGR2 in the OE19 cells. (B) The membrane was stripped and reprobed for β-actin as a western blot control (lanes 1 and 2). Secondary antibody cross-reactivity confirmed the presence of IgG in both IPs (lanes 3 and 4). One representative experiment is shown (N=3). kDa markers are shown on the left. Full length unedited blots are provided as supplementary data.

Figure 6: Co-localisation of AGR2 in OE19 cells.

OE19 cells on coverslips were fixed, permeabilised and stained for the expression and co-localisation of (A) AGR2 and the ER marker PDI; (B) AGR2 and the Golgi marker GM130; (C) AGR2 and Prx-IV; (D) AGR2 and ALDH3A1; (E) AGR2 and MUC-5AC. (F) The distinction between the ER and the cytoskeleton was visualised by co-staining for PDI and tubulin. DAPI was used to stain the nucleus (panel 1; blue) and DIC was used to depict cell morphology (panel 4 in A). AGR2 co-localised with Prx-IV (C) and partially co-localised with ALDH3A1 (D). > = non-ER localisation of ALDH3A1; * = examples of co-staining of AGR2 and ALDH3A1. Images were taken on a Zeiss LSM 880 confocal microscope at x63 magnification. White scale bars represent 10 μm. One representative set of experiments is shown (N=3).

Figure 7: MUC-5AC interacts with AGR2 in esophageal adenocarcinoma

Lysates +/- NEM (A, B) or AGR2 IPs (C) from normal esophageal tissue (N) or adenocarcinoma (T) were analysed by SDS-PAGE and subjected to western blotting with the MUC-5AC antibody (A and C) or were immunoblotted for AGR2 (B). MUC-5AC interacted with AGR2 in the adenocarcinoma tissue only. Coomassie staining was used to verify tissue lysis after Bradford protein analysis (D). Note that tissue specific variations in the levels of GAPDH and actin between normal and adenocarcinoma samples prohibited their use as loading controls. One of two replicates is shown. kDa markers are given on the left. Full length unedited images of (B) are provided as supplementary data.

Figure 8: Expression of AGR2, MUC-5AC, Prx-IV and SQSTM1 in Barrett's Esophagus and adenocarcinoma.

Human tissue sections (4 microns) from Barrett's esophagus (columns 1 and 2) and esophageal adenocarcinoma (columns 3 and 4) were immunohistochemically stained for (A) AGR2; (B) MUC-5AC;

(C) Prx-IV and (D) SQSTM1. Antibody specific staining was visualised by DAB (brown) and counterstaining was with haematoxylin to visualise cell nuclei (blue). Secondary antibodies alone were used as a negative control (columns 2 and 4). The dysplastic goblet cells showed strong staining with all four proteins. All sections were taken from the same Barrett's esophagus block (columns 1 and 2) or adenocarcinoma block (columns 3 and 4). Note that the morphology of the goblet cells changes with sequential sections. A representative staining series is shown (N=3). Stainings of the N2 and N3 tissue sections are shown in the supplementary data. Black scale bars represent 50 μm.

Supplementary Figure 1 (relating to Figure 8): Expression of AGR2, MUC-5AC, Prx-IV and SQSTM1 in Barrett's Esophagus and adenocarcinoma.

Human tissue sections (4 microns) from Barrett's esophagus (columns 1 and 2) and esophageal adenocarcinoma (columns 3 and 4) were immunohistochemically stained for (A) AGR2; (B) MUC-5AC; (C) Prx-IV; (D) SQSTM1 and (E) with eosin to stain the cytoplasm. Antibody specific staining was visualised by DAB (brown) and counterstaining was with haematoxylin to visualise cell nuclei (blue). Secondary antibodies alone were used as a negative control (columns 2 and 4). The dysplastic goblet cells showed strong staining with all four proteins. All sections were taken from the same Barrett's esophagus block (columns 1 and 2) or adenocarcinoma block (columns 3 and 4). These images are from sample set 2. Note that the morphology of the goblet cells changes with sequential sections. Scale bar = 50 μm.

Supplementary Figure 2 (relating to Figure 8): Expression of AGR2, MUC-5AC, Prx-IV and SQSTM1 in Barrett's Esophagus and adenocarcinoma.

Human tissue sections (4 microns) from Barrett's esophagus (columns 1 and 2) and esophageal adenocarcinoma (columns 3 and 4) were immunohistochemically stained for (A) AGR2; (B) MUC-5AC; (C) Prx-IV; (D) SQSTM1 and (E) with eosin to stain the cytoplasm. Antibody specific staining was visualised by DAB (brown) and counterstaining was with haematoxylin to visualise cell nuclei (blue). Secondary antibodies alone were used as a negative control (columns 2 and 4). The dysplastic goblet cells showed strong staining with all four proteins. All sections were taken from the same Barrett's esophagus block (columns 1 and 2) or adenocarcinoma block (columns 3 and 4). These images are from sample set 3. Note that the morphology of the goblet cells changes with sequential sections. Scale bar = 50 μm.

Supplementary Figure 3: Low magnification overview of AGR2 and MUC-5AC co-expression (brown staining) in the dysplastic goblet cells of three independent Barrett's esophagus tissue samples. Nuclei were costained with haematoxlylin (blue). Scale bar = 200 μm.

Supplementary Figure 4: Costaining of AGR2 (brown) with acidic mucins (alcian blue stain). NE = normal esophagus, BE = Barrett's esophagus, EA = esophageal adenocarcinoma. AGR2 and mucins are absent from normal esophageal tissue. Representative image from N=3 stainings. Scale bar = 100 μm.

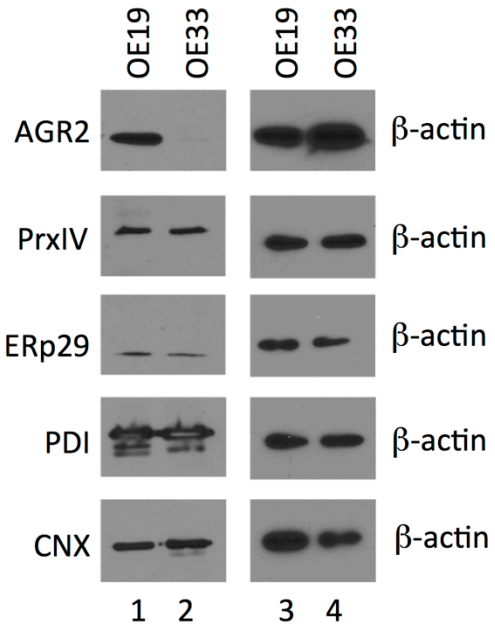
OE19
OE33
OE19
OE33
AGR2
β-actin
PrxIV
β-actin
ERp29
β-actin
PDI
β-actin
CNX
β-actin
1
2
3
4

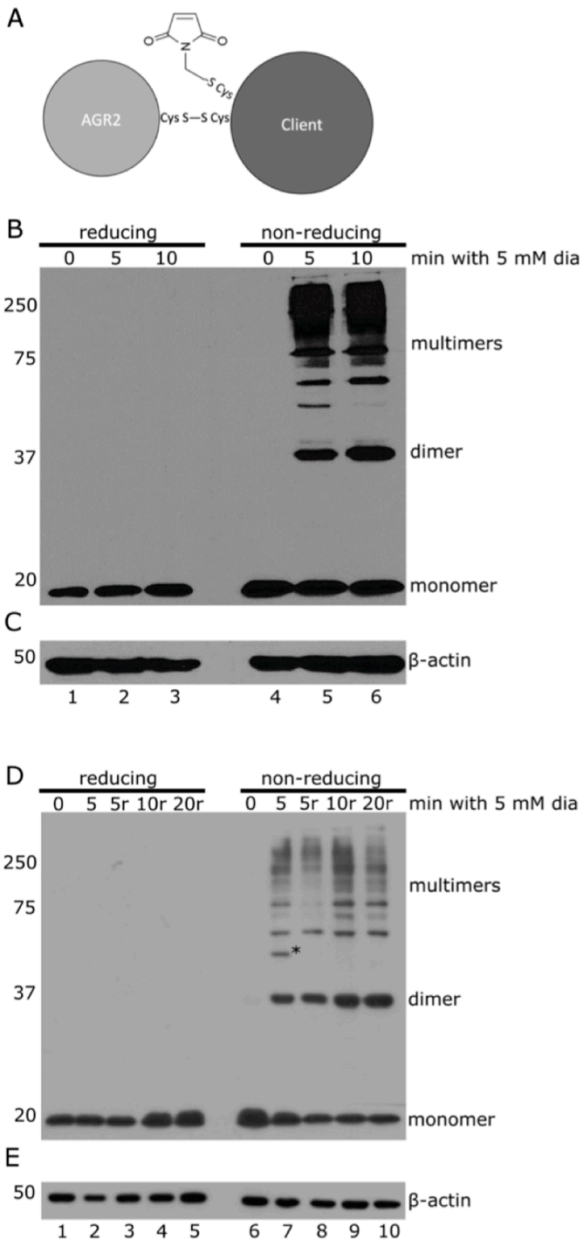
A
AGR2
Cys S—S Cys
Client
B
reducing
non-reducing
0 5 10
0 5 10
min with 5 mM dia
250
75
37
20
multimers
dimer
monomer
C
50
β-actin
1 2 3 4 5 6
D
reducing
non-reducing
0 5 5r 10r 20r
0 5 5r 10r 20r
min with 5 mM dia
250
75
37
20
multimers
*
dimer
monomer
E
50
β-actin
1 2 3 4 5 6 7 8 9 10

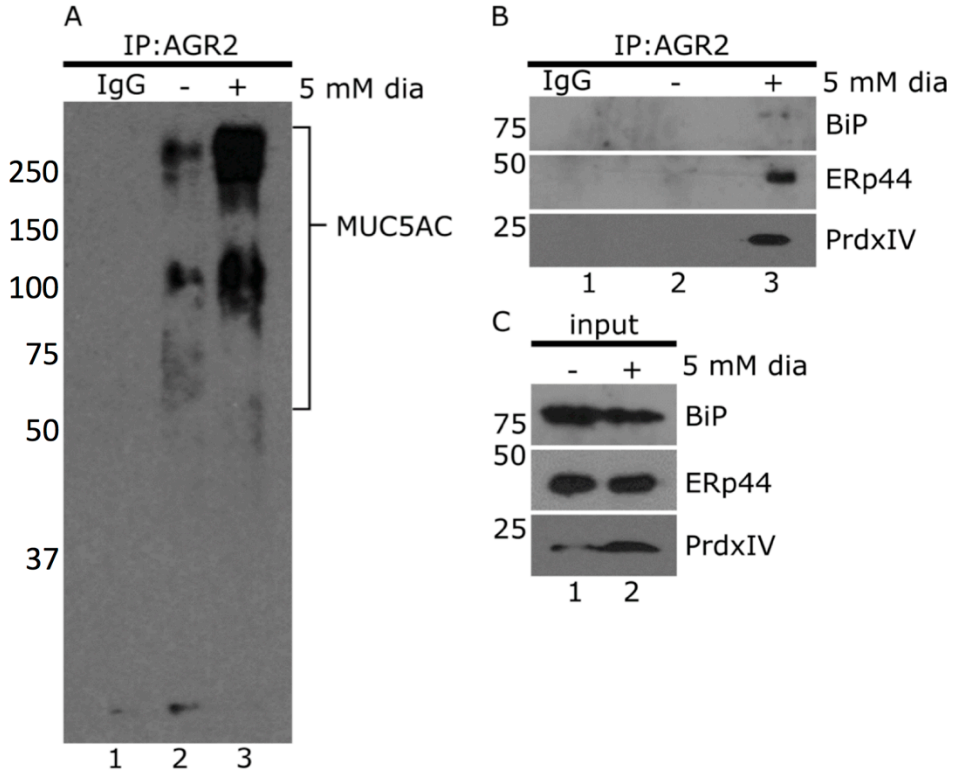
A
IP:AGR2
IgG - +
5 mM dia
250
150
100
75
50
37
MUC5AC
1 2 3
B
IP:AGR2
IgG - +
5 mM dia
75
50
25
BiP
ERp44
PrdxIV
1 2 3
C
input
- +
5 mM dia
75
50
25
BiP
ERp44
PrdxIV
1 2

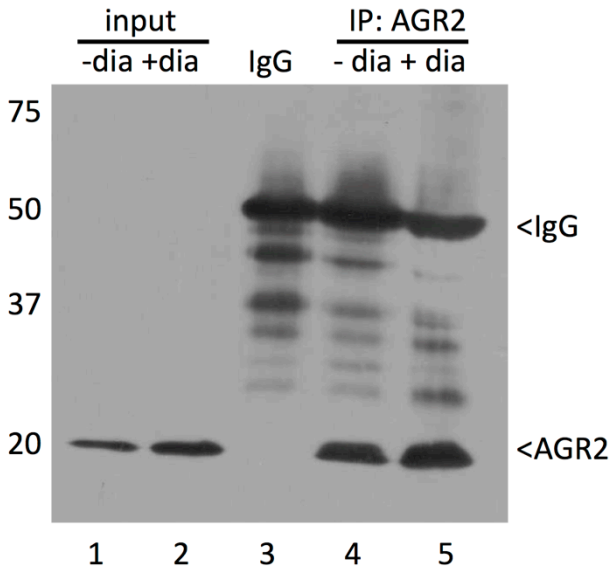
input
-dia +dia
IgG
IP: AGR2
- dia + dia
75
50
37
20
<IgG
<AGR2
1
2
3
4
5

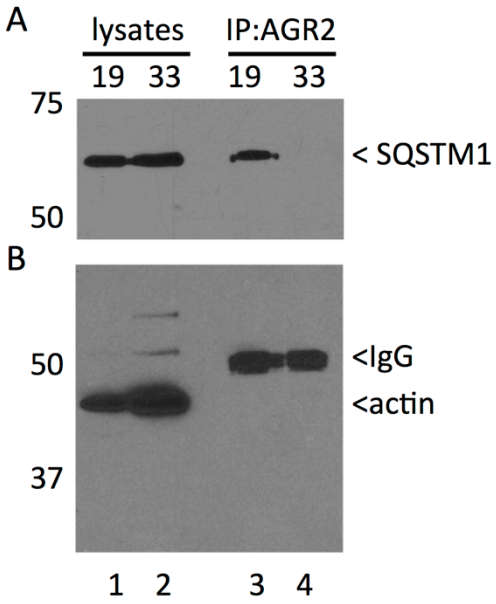
A
lysates
IP:AGR2
19 33 19 33
75
50
< SQSTM1
B
50
37
<IgG
<actin
1 2 3 4

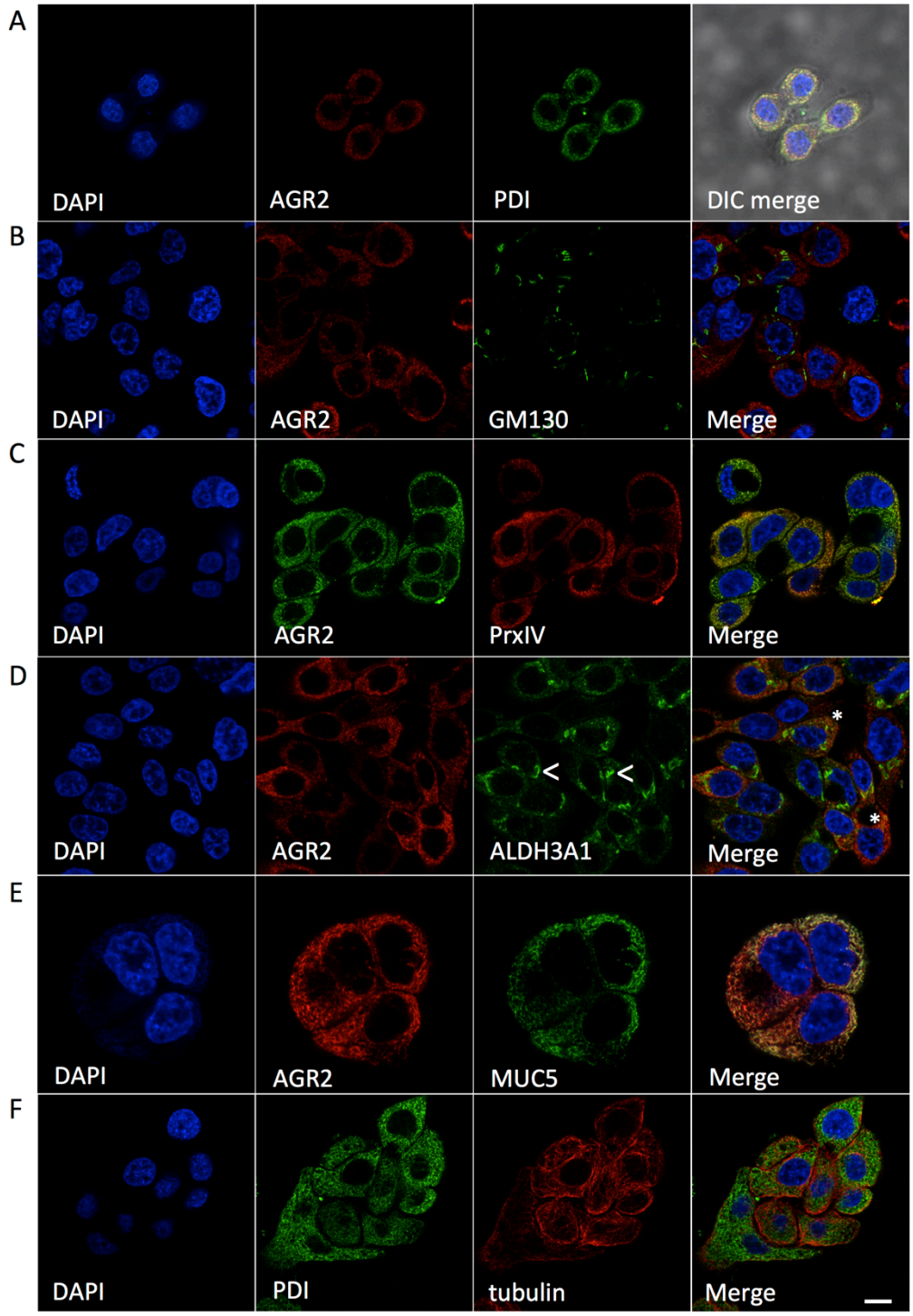
A
DAPI
AGR2
PDI
DIC merge
B
DAPI
AGR2
GM130
Merge
C
DAPI
AGR2
PrxIV
Merge
D
DAPI
AGR2
ALDH3A1
Merge
E
DAPI
AGR2
MUC5
Merge
F
DAPI
PDI
tubulin
Merge

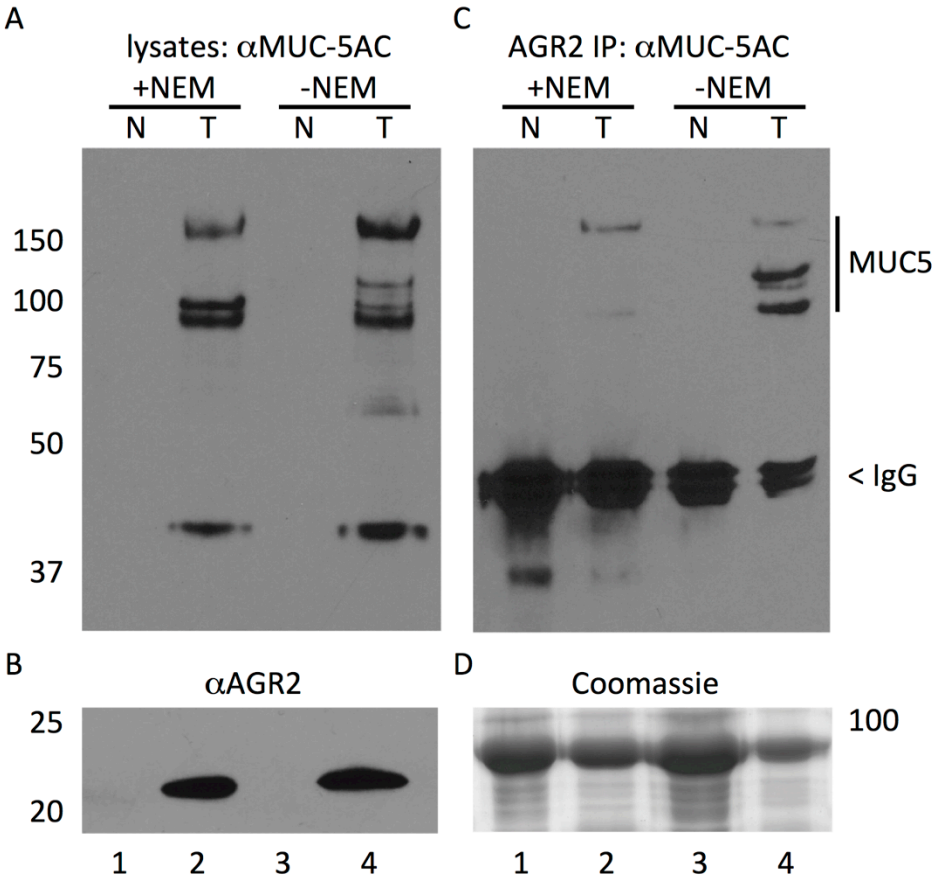
A
lysates: αMUC-5AC
+NEM
-NEM
N T N T
150
100
75
50
37
C
AGR2 IP: αMUC-5AC
+NEM
-NEM
N T N T
MUC5
< IgG
B
αAGR2
25
20
1 2 3 4
D
Coomassie
100
1 2 3 4

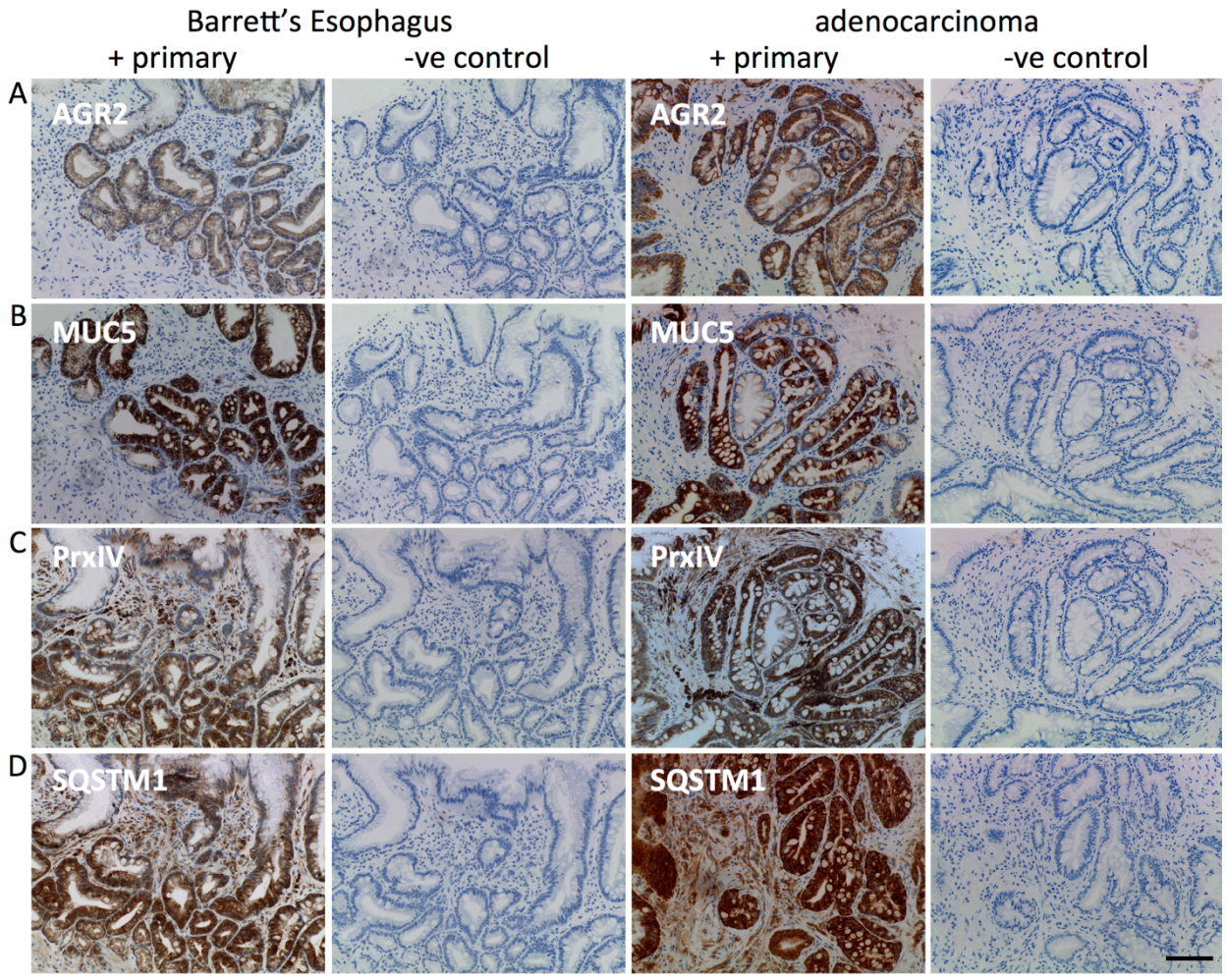
Barrett's Esophagus
+ primary
-ve control
adenocarcinoma
+ primary
-ve control
A
AGR2
AGR2
B
MUC5
MUC5
C
PrxIV
PrxIV
D
SQSTM1
SQSTM1

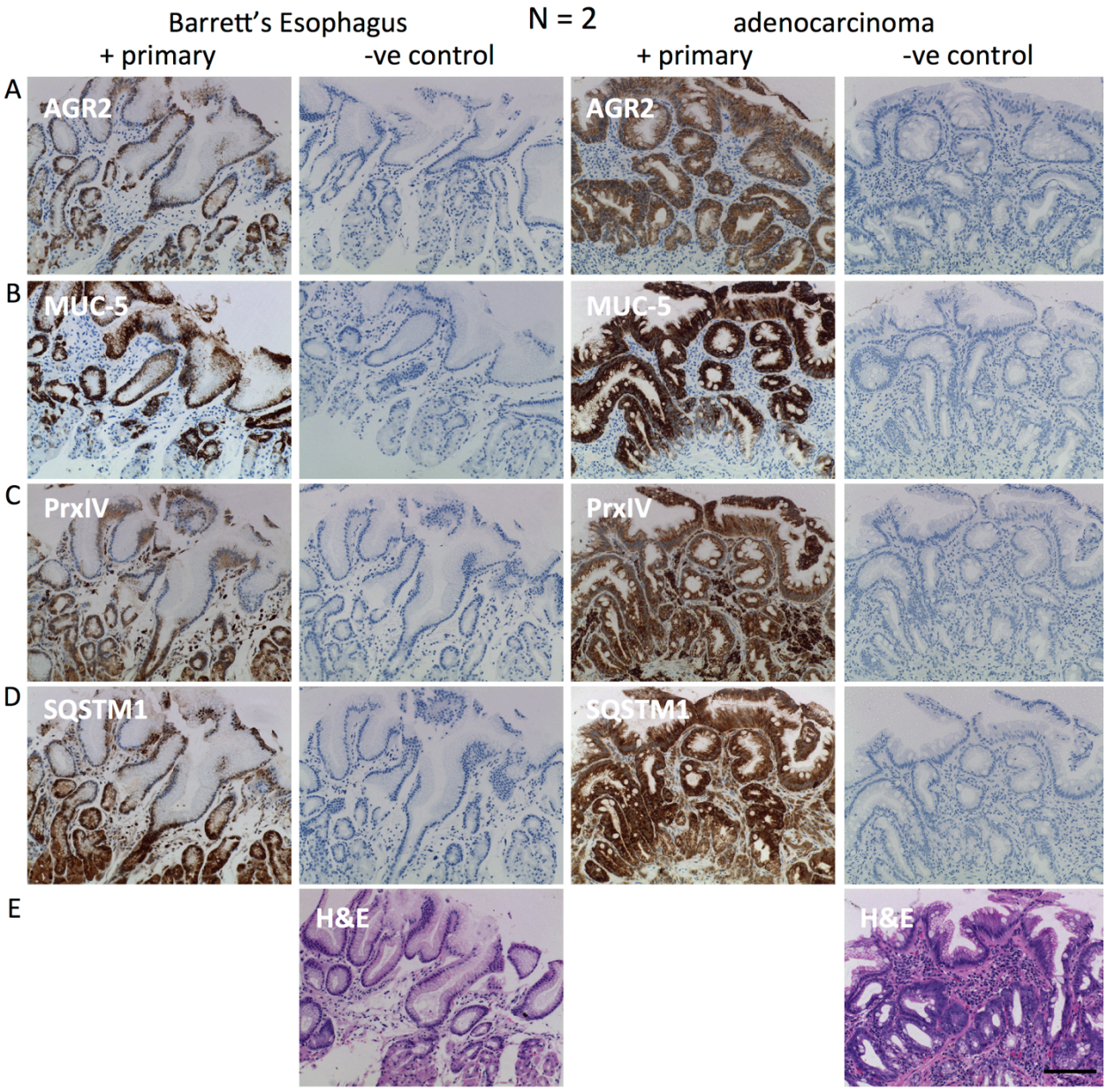

Supplementary Figure 1 (relating to Figure 8):

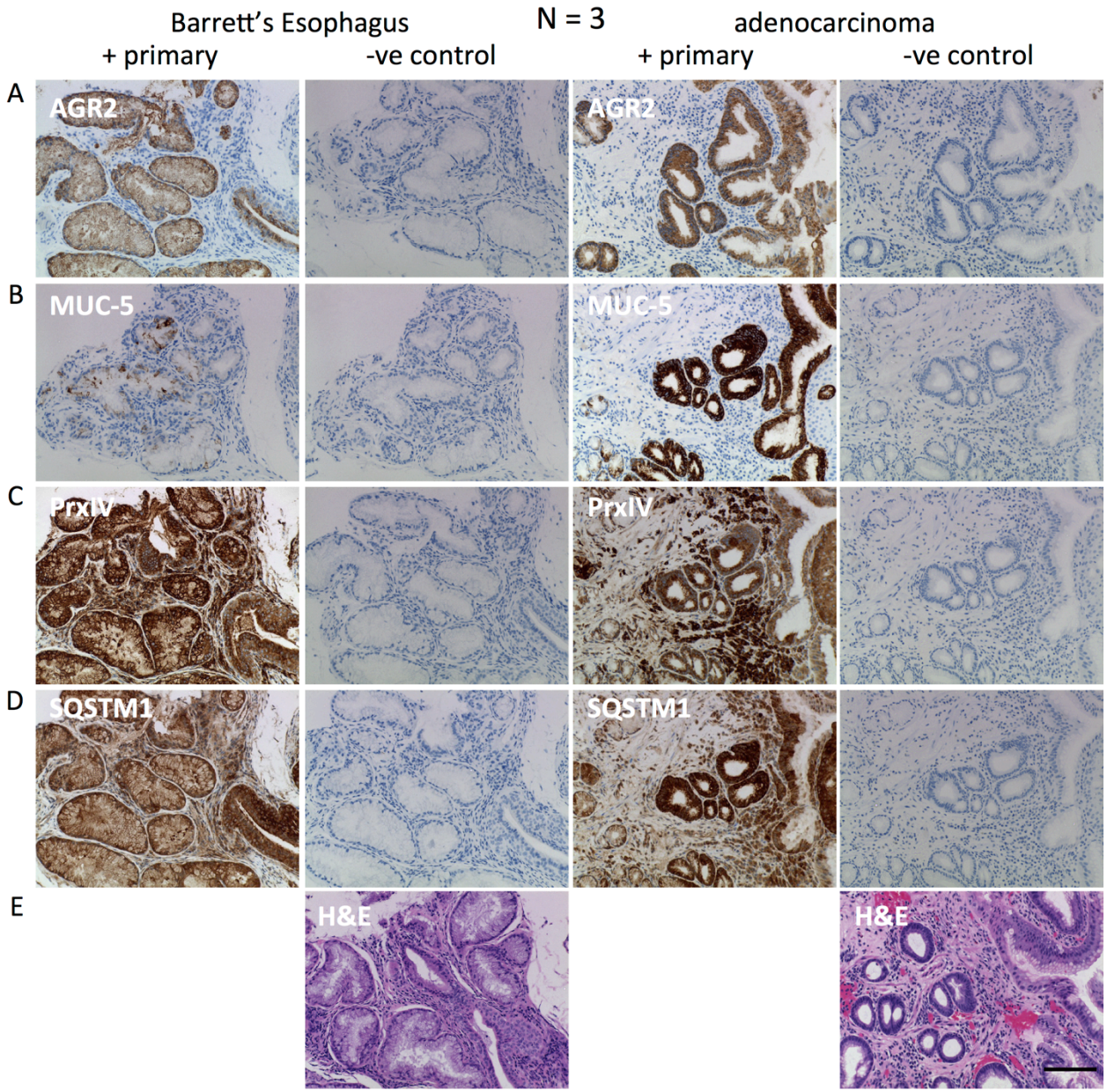

Supplementary Figure 2 (relating to Figure 8):

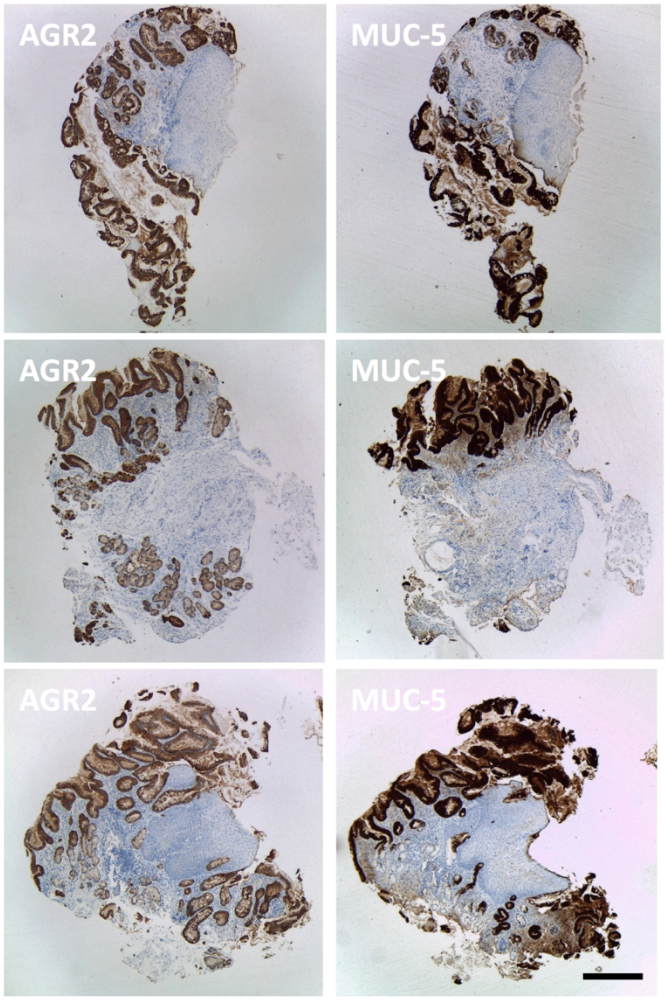

Supplementary Figure 3

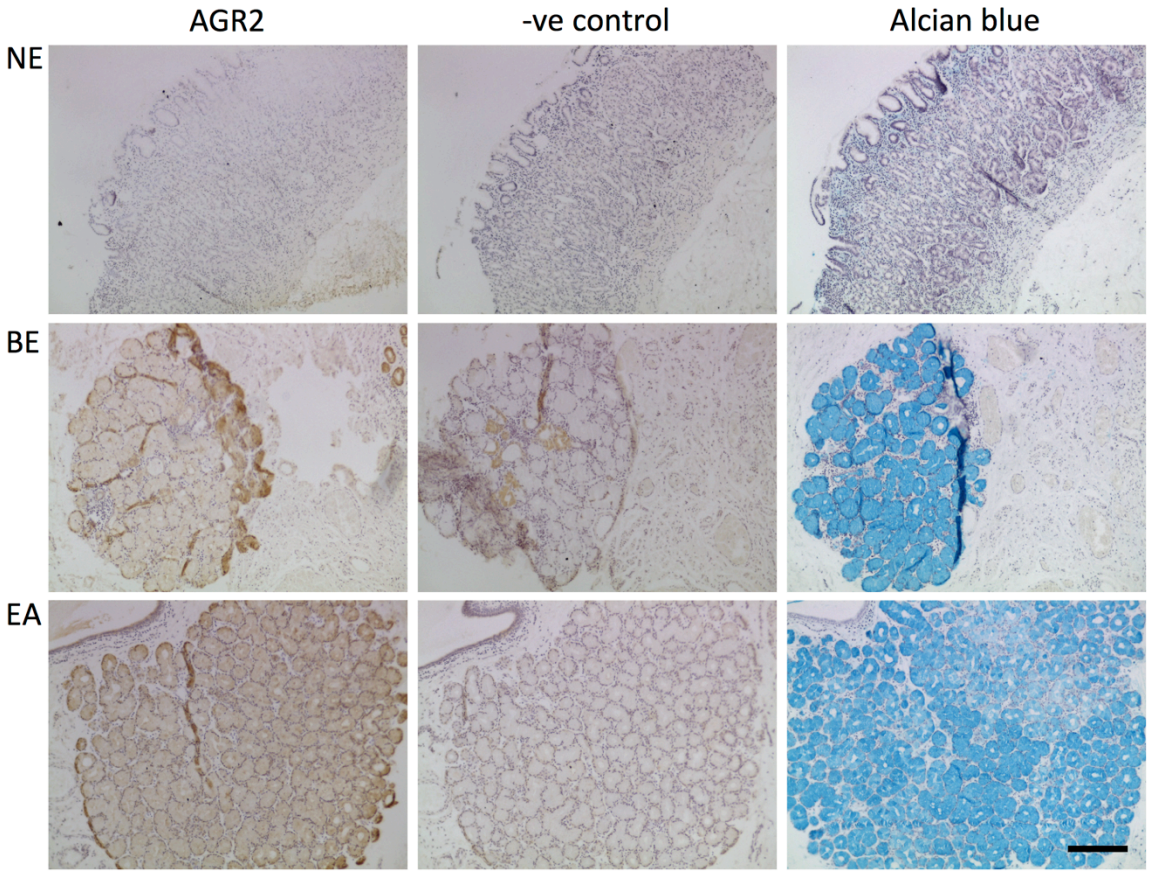

Supplementary Figure 4